RESEARCH ARTICLE OPEN ACCESS

Convective Heat And Mass Transfer Flow Of A Micropolar Fluid In A Rectangular Duct With Soret And Dufour Effects And Heat Sources

C.Sulochana[a], K. Gnanaprasunamba[b]*
[a] Department of Mathematics, Gulberga University, Gulberga, Karnataka, India
[b] Department of Mathematics, SSA Govt. First Grade College, Bellary, Karnataka, India

Abstract
In this chapter we make an investigation of the convective heat transfer through a porous medium in a Rectangular enclosure with Darcy model. The transport equations of liner momentum, angular momentum and energy are solved by employing Galerkine finite element analysis with linear triangular elements. The computation is carried out for different values of Rayleigh number – Ra micropolar parameter – R, spin gradient parameterλ, Eckert number Ec and heat source parameterα. The rate of heat transfer and couple stress on the side wall is evaluated for different variation of the governing parameters.

Keywords: Heat and Mass Transfer, Micropolar Fluid, Soret and Dufour Effect, Rectangular Duct

I. INTRODUCTION

As high power electronic packaging and component density keep increasing substantially with the fast growth of electronic technology, effective cooling of electronic equipment has become exceptionally necessary. Therefore, the natural convection in an enclosure has become increasingly important in engineering applications in recent years. Through studies of the thermal behavior of the fluid in a partitioned enclosure is helpful to understand the more complex processes of natural convection in practical applications Number of studies, numerical and experimental, concerned with the natural convection in an enclosure with or without a divider were conducted in past years.

Several relevant analytical and experimental studies have been reported during the past decades. Excellent reviews have been given by Ostrach [17] and Catton [2]. The critical Rayleigh numbers for natural convection in rectangular boxes heated from below and cooled from above have been obtained theoretically by Davis [7] and Cotton [4]. Samuels and Churchill [20] presented the stability of fluids in rectangular region heated from below and obtained the critical Rayleigh numbers with finite differences approximation. Ozoe et. al., [18,19] determined experimentally and numerically the natural convection in an inclined long channel with a rectangular cross-section, and found the effects of inclination angle and aspect ratio on the circulation and rate of heat transfer, Wilson and Rydin [22] discussed bifurcation phenomenon in a rectangular cavity, as calculated by a nodal integral method. They obtained critical aspect ratios and Rayleigh numbers and found good agreement with the results of Ref [5]. Numerous studies have been presented for a different arrangement of boundary conditions [14-15]. Several analytical studies of natural heat transfer in a rectangular porous cavity have been carried out recently [1, 2]. The theory of micropolar fluids developed by Erigen [8, 9, 11] has been a popular filed of research in recent years. In this theory, the local effects arising from the microstructure and the intrinsic motions of the fluid elements are taken into account. It has been expected to describe properly the non-Newtonian behavior of certain fluids, such as liquid crystals, ferroliquids, colloidal fluid, and liquids with polymer additives. Recently Jena and Bhattacharya [13] studied the effect of microstructure on the thermal convection in a rectangular box heated from below wit Galerkin's method, and obtained critical Rayleigh numbers for various material parameters, Cehn and Hsu [6] considered the effect of mesh size on the thermal convection in an enclosed cavity. Wang et.al., [24] presented the study of the natural convection of micropolar fluids in an inclined rectangular enclosure, HSU et. al., [24] investigated the thermal convection of micropolar fluids in a lid-driven cavity. They reported that the material parameters such as voters viscosity and sin gradient viscosity strongly influence the flow structure and heat transfer. Cha-Kaungchen et. al., [6] have investigated numerically the steady laminar natural convection flow of a micropolar fluid in a rectangular cavity. The angular momentum and energy are solved with the aid of the cubic spline collocation method. Parametric studies of the effects of microstructure on the fluid flow and heat transfer in the enclosure have been performed.

Wang et. al., (23) have investigated natural convection flow of a micropolar fluid in a partially divided rectangular enclosure. The enclosure is partially divided protruding flore of the enclosure. The effect of the highest on the location of the divider is investigated. Also the effects of material parameters or micropolar fluids or the thermal characters, are also studied for different Rayleigh numbers. Tsan – Hsu et. al., (6) have investigated the effects, the characteristic parameters of micropolar fluids on mixed convection in a cavity. The equations are solved with the help of the cubic spin collocation method.

In this chapter we make an investigation of the convective heat transfer through a porous medium in a Rectangular enclosure with Darcy model. The transport equations of liner momentum, angular momentum and energy are solved by employing Galerkine finite element analysis with linear triangular elements. The computation is carried out for different values of Rayleigh number – Ra micropolar parameter – R, spin gradient parameterλ, Eckert number Ec and heat source parameterα. The rate of heat transfer and couple stress on the side wall is evaluated for different variation of the governing parameters.

II. FORMULATION OF THE PROBLEMS

We consider the mixed convective heat and mass transfer flow of a viscous, incompressible, micropolar fluid in a saturated porous medium confined in the rectangular duet whose base length is a and height b. the heat flux on the base and top walls is maintained constant. The Cartesian coordinate system 0(x, y) is chosen with origin on the central axis of the duct and its base parallel to X-axis, we assume that

(i) The convective fluid and the porous medium are everywhere in local thermodynamic equilibrium.
(ii) There is no phase change of the fluid in the medium.
(iii) The properties of the fluid and of the porous medium are homogeneous and isotropic.
(iv) The porous medium is assumed to be closely packed so that Darcy's momentum law is adequate in the porous medium.
(v) The Boussinesq approximation is applicable,

under the assumption the governing equations are given by

$$\frac{\partial u'}{\partial x'}+\frac{\partial v'}{\partial y'}=0 \tag{2.1}$$

$$\frac{-\partial p}{\partial x}-\frac{(\mu+k)}{k_1}u+k\frac{\partial N}{\partial y}=0 \tag{2.2}$$

$$\frac{-\partial p}{\partial y}-\frac{(\mu+k)}{k_1}v-k\frac{\partial N}{\partial y}-\rho\bar{g}=0 \tag{2.3}$$

$$\rho_\sigma C_P\left[u'\frac{\partial T'}{\partial x}v'\frac{\partial T'}{\partial y'}\right]=k_f\left[\frac{\partial^2 T'}{\partial x'^2}+\frac{\partial^2 T'}{\partial y'^2}\right] \tag{2.4}$$

$$\rho_j\left[u'\frac{\partial N}{\partial x'}+v'\frac{\partial N}{\partial y'}\right]=\gamma\left[\frac{\partial^2 N}{\partial x'^2}+\frac{\partial^2 N}{\partial y'^2}\right]+K\left(\frac{\partial v}{\partial x}-\frac{\partial u}{\partial y}-2N\right) \tag{2.5}$$

$$\rho_\sigma C_P\left[u'\frac{\partial C}{\partial x}v'\frac{\partial C}{\partial y'}\right]=D_m\left[\frac{\partial^2 C}{\partial x'^2}+\frac{\partial^2 C}{\partial y'^2}\right] \tag{2.6}$$

$$\rho'=\rho_0\{1-\beta_0(T-T_0)-\beta^{\bullet}(C-C_0)\}$$

$$T_0=\frac{T_h+T_c}{2},\qquad C_0=\frac{C_h+C_c}{2} \tag{2.7}$$

where u′ and v′ are Darcy velocities along 0(x, y) direction. T′, N, p′ and g′ are the temperature, micro rotation, pressure and acceleration due to gravity, T_c and T_h are the temperature on the cold and warm side walls respectively. ρ′, μ, v and β are the density, coefficients of viscosity, kinematic viscosity and thermal expansion of the fluid, k_1 is the permeability of the porous medium, γ, k are the micropolar and material constant pressure , Q is the strength of the heat source,k11&k2
is the cross diffusivities,γ1 is the chemical reaction parameter,
The boundary conditions are

u′ = v′ = 0 on the boundary of the duct

$T' = T_h$,$C=C_h$ on the side wall to the right (x = 1)
$T' = T_c$,$C=C_c$ on the side wall to the right (x = 0) (2.7)

$$\frac{\partial T'}{\partial y} = 0, \frac{\partial C}{\partial y} = 0$$ on the top (y = 0) and bottom

u = v = 0 walls (y = 0) which are insulated,

$$N = \frac{-1}{2}\frac{\partial u}{\partial x} \text{ On y = 0 \& 1}$$
$$N = \frac{-1}{2}\frac{\partial v}{\partial x} \text{ On x = 0 \& 1} \qquad (2.8)$$

Eliminating the pressure p from equations (2.2) & (2.3) and using (2.6) we get

$$0 = \frac{-(\mu + k)}{k_1}\left(\frac{\partial u}{\partial y} - \frac{\partial v}{\partial x}\right) + k\left(\frac{\partial^2 u}{\partial y^2} - \frac{\partial^2 v}{\partial x^2}\right) + \rho\beta g(\frac{\partial}{\partial x}(T - T_0) + \rho\beta^{\bullet} g\frac{\partial}{\partial x}(C - C_0) \quad (2.11)$$

On introducing the stream functionψ, as

$$u = -\frac{\partial \Psi}{\partial y}, \qquad v = \frac{\partial \Psi}{\partial y}$$

the equations (2.11) & (2.5) reduce to

$$\frac{(\mu + k)}{k_1}\nabla^2\Psi + k\nabla^2 N + (\beta_0 g\frac{\partial}{\partial x}(\mathrm{T} - \mathrm{T}_0) + \beta^{\bullet} g\frac{\partial}{\partial x}(\mathrm{C} - \mathrm{C}_0)) \qquad (2.12)$$

$$\rho_0 C_P\left(\frac{\partial \Psi}{\partial x}\frac{\partial T}{\partial y} - \frac{\partial \Psi}{\partial y}\frac{\partial T}{\partial y}\right) = k_f \nabla^2 T \quad (2.13)$$

$$\rho_j\left(\frac{\partial \psi}{\partial x}\frac{\partial \psi}{\partial y} - \frac{\partial \psi}{\partial y}\frac{\partial \psi}{\partial x}\right) = \gamma\nabla^2 N + K\left(\nabla^2\psi - 2N\right) \qquad (2.14)$$

$$\left(\frac{\partial \Psi}{\partial x}\frac{\partial C}{\partial y} - \frac{\partial \Psi}{\partial y}\frac{\partial C}{\partial y}\right) = D_m\nabla^2 C \qquad (2.15)$$

Now introducing the following non-dimensional variables

$$x' = ax: \qquad y' = by: \qquad C = \frac{b}{a}, \quad \Psi' = \frac{\Psi}{\nu}$$

$$u' = \left(\frac{\nu}{a}\right)u: \qquad v' = \left(\frac{\nu}{a}\right)v: \qquad p' = \left(\frac{\nu^2\rho}{a^2}\right)p$$

$T' = T_c + \theta(T_h - T_c)$: $\qquad N' = \left(\frac{N}{\frac{\nu}{a^{22}}}\right)$

$C' = C_c + C\,(C_h - C_c)$: (2.16)

the equations (2.12) – (2.14) in the non-dimensional form are

$$\nabla\ \psi = -RD^{-1}\nabla^2\omega - GD^{-1}(\frac{\partial\theta}{\partial x} + N\frac{\partial C}{\partial x}) \qquad (2.17)$$

$$P\left[\frac{\partial\Psi}{\partial x}\frac{\partial\theta}{\partial y}-\frac{\partial\Psi}{\partial y}\frac{\partial\theta}{\partial y}\right]=\left[\frac{\partial^2\theta}{\partial x^2}+N_2\frac{\partial^2\theta}{\partial y^2}\right] \tag{2.18}$$

$$\nabla^2\omega+2\left(\frac{R}{\lambda}\right)\omega=\left(\frac{R}{\lambda}\right)\nabla^2\Psi \tag{2.19}$$

$$Sc\left[\frac{\partial\Psi}{\partial x}\frac{\partial C}{\partial y}-\frac{\partial\Psi}{\partial y}\frac{\partial C}{\partial y}\right]=\left[\frac{\partial^2 C}{\partial x^2}+\frac{\partial^2 C}{\partial y^2}\right] \tag{2.20}$$

where

$G=\dfrac{g\beta(T_h-T_c)a^3}{\nu^2}$ (Grashof number)

$P=\mu C_p/k_f$ (Prandtl number)

$D^{-1}=\dfrac{a^2}{k_1}$ (Darcy parameter)

$R=\dfrac{k}{\mu}$ (Micropolar parameter)

$\lambda=\dfrac{\gamma}{\nu a^2}$ (Micropolar material constant)

$Sc=\dfrac{\nu}{D_m}$ (Schmidt number)

$N=\dfrac{\beta^{\bullet}(C_h-C_c)}{\beta(T_h-T_c)}$ (Buoyancy ratio)

And the corresponding boundary conditions are

$\psi_y=\psi_x=0$ on the boundary (2.18a)

$\theta=1$, C=1 on x = 1 (2.18b)

$\theta=0$, C=0 on x = 0 (2.18b)

$N=\dfrac{1}{2}\dfrac{\partial^2\Psi}{\partial x\partial y}$ On y = 0 & 1

$N=-\dfrac{1}{2}\dfrac{\partial^2\Psi}{\partial y\partial x}$ On x = 0 & 1 (2.18c)

III. FINITE ELEMENT ANALYSIS AND SOLUTION OF THE PROBLEM

The region is divided into a finite number of three noded triangular elements, in each of which the element equation is derived using Galerkin weighted residual method. In each element f_i the approximate solution for an unknown f in the variation formulation is expressed as a linear combination of shape function $\left(N_k^i\right)$k = 1, 2, 3, which are linear polynomials sin x and y. This approximate solution of the unknown f coincides with actual values of each node of the element. The variation formulation results in 3x3 matrix equation (stiffness matrix) for the unknown local nodal values of the given element. The stiffness matrices are assembled in terms of global nodal values using inter element continuity and boundary conditions resulting in global matrix equation.

In each case there are r district global nodes in the finite element domain and f_p = (p =1, 2.r) is the global nodal values of any unknown f defined over the domain

Then $f = \sum_{\propto=1}^{s} \sum_{p=1}^{r} f_p \phi'_p$

Where the first summation denotes summation over s elements and the second one represents summation over the independent global nodes and

$\phi_p^i = N_N^i$, if p is one of the

Local nodes say k of the element $e_i = 0$,

f'_p s are determined from the global matrix equation. Based on these lines we now make a finite element analysis of the given problem governed by (2.15) – (2.17) subject to the conditions (2.18a) – (2.18c).

Let ψ^i, θ^i and N^i be the approximate valuesψ, θ and N in a element e_i

$$\Psi^i = N_1^i \Psi_1^i + N_2^i \Psi_2^i + N_3^i \Psi_3^i \quad (3.1a)$$

$$\theta^i = N_1^i \theta_1^i + N_2^i \theta_2^i + N_3^i \theta_3^i \quad (3.1b)$$

$$C^i = N_1^i C_1^i + N_2^i C_2^i + N_3^i C_3^i \quad (3.1c)$$

$$N = N_1^i i + N_2^i N^i + N_3^i N^i \quad (3.1d)$$

Substituting the approximate value ψ^i θ^I, C^i and ω^i forψ, θ, C and ω respectively in (2.15)

$$E_1^i = \left(\frac{\partial^2 \theta^i}{\partial x^2} \right) + \frac{\partial^2 \theta^i}{\partial y^2} - P\left[\frac{\partial \Psi^i}{\partial y} \frac{\partial \theta^i}{\partial x} - \frac{\partial \Psi^i}{\partial x} \frac{\partial \theta^i}{\partial y} \right] \quad (3.2)$$

$$E_2^i = \frac{\partial^2 \omega^i}{\partial x^2} + \frac{\partial^2 \omega^i}{\partial y^2} + 2R\omega^i - \frac{R}{\lambda}\left(\frac{\partial^2 \Psi^i}{\partial x^2} + \frac{\partial^2 \Psi^i}{\partial y^2} \right) \quad (3.3)$$

Under Galaerkin method this is made orthogonal over the domain e_i to the respective shape functions (weight function)

Where $\int_{e_i} E_1^i N_k^i d\Omega = 0$

$$\int_{e_i} E_2^i N_k^i d\Omega = 0$$

$$(3.4) \Rightarrow \int_{e_i} N_k^u \left(\frac{\partial^2 \theta^i}{\partial x^2} \right) + \frac{\partial^2 \theta^i}{\partial y^2} + P\left[\frac{\partial \Psi^i}{\partial y} \frac{\partial \theta^i}{\partial x} - \frac{\partial \Psi^i}{\partial x} \frac{\partial \theta^i}{\partial y} \right]^i) d\Omega = 0$$

$$\int_{e_i} N_k^i \left[\frac{\partial^2 \omega^i}{\partial x^2} + \frac{\partial^2 \omega^i}{\partial y^2} \right] + 2R\omega^i - \frac{R}{\lambda}\left(\frac{\partial^2 \Psi^i}{\partial x^2} + \frac{\partial^2 \Psi^i}{\partial y^2} \right) d\Omega = 0 \quad (3.5)$$

Using Greeen's theorem we reduce the surface integral (3.4) & (3.5) without affecting ψ terms and obtain

$$\int_{e_i} N_k^i \left\{ \left(1 + \frac{4}{3N} \right) \frac{\partial N_k^i}{\partial x} \frac{\partial \theta^i}{\partial x} + \frac{\partial N_k^i}{\partial y} \frac{\partial \theta^i}{\partial y} - PN_k \left[\frac{\partial \Psi^i}{\partial y} \frac{\partial \theta^i}{\partial x} - \frac{\partial \Psi^i}{\partial x} \frac{\partial \theta^i}{\partial y} \right] \right\} d\Omega$$

$$= \int_{\Gamma_i} N_k^i \left(\frac{\partial \theta^i}{\partial x} nx + \frac{\partial \theta^i}{\partial x} ny \right) d\Gamma_i \quad (3.6)$$

$$\int_{e_i e_i} N_k^i \left\{ \frac{\partial N_k^i}{\partial x} \frac{\partial \omega^i}{\partial x} + \frac{\partial N_k^i}{\partial y} \frac{\partial \omega^i}{\partial y} \right\} + 2R\omega^i - \frac{R}{\lambda}\left(\frac{\partial N_k^i}{\partial x} \frac{\partial \Psi^i}{\partial x} + \frac{\partial N_k^i}{\partial y} \frac{\partial \Psi^i}{\partial y} \right)$$

$$= \int_{e_i} N_k^i \left[\left(\frac{\partial \omega^i}{\partial x} - \frac{R}{\lambda} \frac{\partial \Psi^i}{\partial x} \right) nx + \left(\frac{\partial \omega^i}{\partial y} - \frac{R}{\lambda} \frac{\partial \Psi^i}{\partial y} \right) ny + \right] d\Gamma_i \qquad (3.7)$$

Where Γ_1 is the boundary of e_i, substituting L.H.S of (3.1a) – (3.1c) for ψ^i, θ^i and N^i in (3.6) & (3.7) we get

$$\sum_{i=1}^{3} \int_{e_i} \left(1 + \frac{4}{3N_1} \right) \frac{\partial N_k^i}{\partial x} \frac{\partial N_L^i}{\partial x} - \frac{\partial N_L^i}{\partial y} \frac{\partial N_k^i}{\partial y}$$

$$- P_1 \sum_{i=1}^{3} \Psi_m^i \int_{e_i} \left[\frac{\partial N_m^i}{\partial y} \frac{\partial N_L^i}{\partial x} - \frac{\partial N_m^i}{\partial x} \frac{\partial N_L^i}{\partial y} \right]$$

$$= \int_{\Gamma_i} N_k^i \left[\frac{\partial \theta^i}{\partial x} nx + \frac{\partial \theta^i}{\partial y} ny \right] d\Gamma_i = W_k^i$$

(l, m, k = (1, 2, 3) (3.8)

$$\sum_{i=1}^{3} \int_{e_i} \frac{\partial N_k^i}{\partial x} \frac{\partial N_L^i}{\partial x} - \frac{\partial N_L^i}{\partial y} \frac{\partial N_k^i}{\partial y}$$

$$- Sc \sum_{i=1}^{3} \Psi_m^i \int_{e_i} \left[\frac{\partial N_m^i}{\partial y} \frac{\partial N_L^i}{\partial x} - \frac{\partial N_m^i}{\partial x} \frac{\partial N_L^i}{\partial y} \right]$$

$$- k_c \Sigma C^i \int_{e_i} N_k^i N_l^i d\Omega_i + ScSr \sum_{ei} \theta^i \left(\frac{dN_k^i}{dx} \frac{dN_L^i}{dx} + \frac{dN_m^i}{dx} \frac{dN_L^i}{dx} \right) d\Omega = 0$$

$$= \int_{\Gamma_i} N_k^i \left[\left(\frac{\partial \theta^i}{\partial x} nx + \frac{\partial \theta^i}{\partial y} ny \right] d\Gamma_i = W_k^i \right.$$

(l, m, k = (1, 2, 3)

$$\sum_{1} \int_{e_i} N^i \left(\frac{\partial N_k^i}{\partial x} \frac{\partial N_L^i}{\partial y} + \frac{\partial N_L^i}{\partial y} \frac{\partial N_k^i}{\partial y} \right)$$

$$+ \frac{2R}{\lambda} \Sigma \omega^i \int N_k^i N_L^i d\Omega - \frac{R}{\lambda} \Sigma \Psi^i \int \left(\frac{\partial N_k^i}{\partial x} \frac{\partial N_J^i}{\partial x} + \frac{\partial N_k^i}{\partial y} \frac{\partial N_J^i}{\partial y} \right) d\Omega \qquad (3.9)$$

$$= \int_{\Gamma_i} N_k^i \left[\left(\frac{\partial \omega^i}{\partial x} - \frac{R}{\lambda} \frac{\partial \Psi^2}{\partial x} \right) nx + \left(\frac{\partial \omega^i}{\partial y} - \frac{R}{\lambda} \frac{R \partial \Psi^i}{\partial y} \right) ny \right] d\Gamma_i = Q_i^N$$

Where $Q_k^i = Q_{k1}^i + Q_{k2}^i + Q_{k3}^i, Q_k^i{}'s$ being the values of Q_k^i on the sides s = (1, 2, 3) of the element e_i. The sign of Q_k^i 's depends on the direction of the outward normal with reference to the element.

Choosing different N_k^i 's as weight functions and following the same procedure we obtain matrix equations for three unknowns (Q_p^i)

$$(Q_p^i)(Q_p^i) = (Q_k^i) \qquad (3.10)$$

Where (Q^i_{pk}) 3 x 3 matrixes are, $(Q^i_p),(Q^i)$ are column matrices.

Repeating the above process with each of s elements, we obtain sets of such matrix equations. Introducing the global coordinates and global values for (Q^i_p) and making use of inter element continuity and boundary conditions relevant to the problem the above stiffness matrices are assembled to obtain a global matrix equation. This global matrix is rxr square matrix if there are r distinct global nodes in the domain of flow considered.

Similarly substituting ψ^i θ^i ,ω^i , and ϕ^i in (2.12) and defining the error and following the Galerkin method we obtain using Green's Theorem, (3.8) reduces to

$$\int_\Omega \left[\frac{\partial N^i_k}{\partial x}\frac{\partial \Psi^i}{\partial x} + \frac{\partial N^i_k}{\partial y}\frac{\partial \Psi^i}{\partial y} + GD^{-1}\frac{\partial N^i_k}{\partial x} + \frac{RD^{-1}}{\lambda}.\left(\frac{\partial N^i_k}{\partial x}\frac{\partial N^i}{\partial x} + \frac{\partial N^i_k}{\partial y}\frac{\partial N^i}{\partial y} \right) \right] d\Omega$$

$$= \int_\Gamma \left(\frac{\partial \Psi^i}{\partial x}nx + \frac{\partial \Psi^i}{\partial y}ny \right) d\Gamma + RD^{-1}\int_\Gamma N^i_k \left(\frac{\partial \Psi^i}{\partial x}ny + \frac{\partial N^i}{\partial y}ny \right) d\Gamma \qquad (3.9)$$

$$+ GD^{-1}\int_\Gamma N^i_k nx d\Gamma$$

in obtaining (3.9) the Green's Theorem is applied with reference to derivatives of Ψ without affecting θ terms.

Using (3.1-3.1c) in (3.9) we have

$$\sum_m \Psi^i_m \left\{ \int_\Omega \left(\frac{\partial N^i_k}{\partial x}\frac{\partial N^i_m}{\partial x} + \frac{\partial N^i_m}{\partial y}\frac{\partial N^i_k}{\partial y} \right) d\Omega + GD^{-1}\left(\sum_L \theta^i_L \int_\Omega N^i_k \frac{\partial N^i_L}{\partial x} d\Omega + 2\gamma(\theta^i_L)^2 \int_\Omega (N^i_k)^2 \frac{\partial N^i_L}{\partial x} d\Omega \right) \right\}$$

$$= \int N^i_k \left[\left(\frac{\partial \Psi^i}{\partial x} + \frac{\partial N^i}{\partial x} \right) nx + \left(\frac{\partial \Psi^i}{\partial y} + \frac{\partial N^i}{\partial y} \right) ny \right] d\Gamma + \int N^i_k \theta^i d\Omega_i = \Gamma ki \qquad (3.10)$$

In the problem under consideration, for computational purpose, we choose uniform mesh of 10 triangular elements. The domain has vertices whose global coordinates are (0, 0), (1, 0) and (1, c) in the non-dimensional form. Let e_1, e_2…..e_{10} be the ten elements and let θ_1, θ_2,….θ_{10} be the global values of θ and ψ_1, ψ_2 ….ψ_{10} are the global values of ψ at the global nodes of the domain.

IV. SHAPE FUNCTIONS AND STIFFNESS MATRICES

$$\overset{n}{1,1} = 1 - 3x \qquad \overset{n}{1,2} = 3x - \frac{3y}{h}$$

$$\overset{n}{2,1} = 1 - \frac{3y}{h} \qquad \overset{n}{2,2} = -1 + \frac{3y}{h}$$

$$\overset{n}{2,3} = 1 - 3x + \frac{3y}{h} \qquad \overset{n}{3,1} = 2 - 3x$$

$$\overset{n}{3,2} = -1 + 3x + \frac{3y}{h} \qquad \overset{n}{3,3} = -\frac{3y}{h}$$

$$\overset{n}{4,1} = 1 - \frac{3y}{C} \qquad \overset{n}{4,2} = -2 + 3x$$

$$\overset{n}{4,3} = 2 - 3x + \frac{3y}{h} \qquad \overset{n}{5,1} = 2 - 3x$$

$$n_{5,2} = -1 + 3x - \frac{3y}{h} \qquad n_{5,3} = \frac{3y}{h}$$

$$n_{6,3} = 1 + \frac{3y}{h} \qquad n_{7,1} = 2 - \frac{3y}{h}$$

$$n_{7,2} = -2 + 3x \qquad n_{7,3} = 1 - 3x + \frac{3y}{h}$$

$$n_{8,1} = 3 - 3x \qquad n_{8,2} = -1 + 3x - \frac{3y}{h}$$

$$n_{9,2} = 3x - \frac{3y}{h} \qquad n_{9,3} = -1 + \frac{3y}{h}$$

The global matrix for θ is

$$A_3 X_3 = B_3 \tag{4.1}$$

The global matrix for N is

$$A_4 X_4 = B_4 \tag{4.2}$$

The global matrix ψ is

$$A_5 X_5 = B_5 \tag{4.3}$$

where

$$A3 = \begin{pmatrix}
-1 & 0 & 0 & 0 & 0 & 0 & -\frac{cR}{216} & 0 & 0 & 0 \\
0 & -1 & 0 & 0 & 0 & -\frac{cR}{108} & -\frac{1}{c^2} + \frac{R}{27c^2} - \frac{R}{12c} & 0 & 0 & 0 \\
0 & 0 & -1 & 0 & 0 & -\frac{1}{c^2} + \frac{R}{27c^2} - \frac{R}{36c} - \frac{cR}{18} & 0 & 0 & 0 & 0 \\
0 & 0 & 0 & -1 & 0 & 0 & 0 & 0 & 0 & 0 \\
0 & 0 & 0 & 0 & -1 & -2 + C - \frac{R}{27} + \frac{R}{18c} + \frac{cR}{108} & 0 & 0 & 0 & 0 \\
0 & 0 & 0 & 0 & 0 & 2 + \frac{1}{c^2} + \frac{1}{c} - \frac{2R}{27} - \frac{R}{27c^2} + \frac{R}{18c} - \frac{7cR}{27} & -2 + C - \frac{R}{27} + \frac{R}{18c} + \frac{cR}{108} & -\frac{1}{c^2} + \frac{R}{18} + \frac{R}{27c^2} - \frac{R}{12c} - \frac{2cR}{27} & 0 & 0 \\
0 & 0 & 0 & 0 & 0 & -C + \frac{11cR}{108} & \frac{1}{c} + C - \frac{35cR}{108} & \frac{19cR}{216} & 0 & 0 \\
0 & 0 & 0 & 0 & 0 & -\frac{1}{c} + \frac{5cR}{108} & \frac{11cR}{216} & \frac{1}{c} + C - \frac{37cR}{108} & 0 & 0 \\
0 & 0 & 0 & 0 & 0 & \frac{R}{9} - \frac{R}{36c} - \frac{cR}{54} & 0 & -2 + C - \frac{7R}{27} + \frac{R}{9c} + \frac{11cR}{108} & -1 & 0 \\
0 & 0 & 0 & 0 & 0 & 0 & 0 & \frac{cR}{8} & 0 & -1
\end{pmatrix}$$

$$A4 = \begin{pmatrix}
-1 & e21 & 0 & 0 & 0 & 0 & e71 & 0 & 0 & 0 \\
0 & e22 & e23 & 0 & 0 & e26 & e27 & 0 & 0 & 0 \\
0 & e32 & e33 & 0 & 0 & e36 & 0 & 0 & 0 & 0 \\
0 & 0 & e43 & -1 & 0 & 0 & 0 & 0 & 0 & 0 \\
0 & 0 & e53 & 0 & e55 & e56 & 0 & 0 & 0 & 0 \\
0 & e62 & e63 & 0 & 0 & e66 & e67 & e68 & 0 & 0 \\
0 & e72 & 0 & 0 & 0 & -c & e77 & e78 & 0 & 0 \\
0 & 0 & 0 & 0 & 0 & e86 & e87 & e88 & 0 & 0 \\
0 & 0 & 0 & 0 & 0 & e96 & 0 & e98 & -1 & 0 \\
0 & 0 & 0 & 0 & 0 & 0 & 0 & -\frac{P\psi}{2} & 0 & -1
\end{pmatrix}$$

$$A5 = \begin{pmatrix} -1 & -\frac{c}{2} & 0 & 0 & 0 & 0 & 0 & 0 & 0 & 0 \\ -1+\frac{c}{2} & 1+\frac{1}{c^2} & -\frac{c}{2} & 0 & 0 & 0 & -\frac{1}{c^2} & 0 & 0 & 0 \\ 0 & -1+\frac{c}{2} & 1+\frac{1}{c^2} & -\frac{c}{2} & 0 & -\frac{1}{c^2} & 0 & 0 & 0 & 0 \\ 0 & 0 & -\frac{18c^2-9c^3}{18c^2} & -\frac{-18+9c-18c^2+9c^3}{18c^2} & -\frac{18-9c}{18c^2} & 0 & 0 & 0 & 0 & 0 \\ 0 & 0 & 0 & -\frac{1}{2c} & 2+\frac{1}{c^2}-c & -2+c & 0 & 0 & -\frac{1}{c^2}+\frac{1}{2c} & 0 \\ 0 & 0 & -\frac{1}{c} & 0 & -c & 2+\frac{1}{c^2}+\frac{1}{c} & -2+c & -\frac{1}{c^2} & 0 & 0 \\ 0 & -\frac{1}{c} & 0 & 0 & 0 & -c & \frac{1}{c}+c & 0 & 0 & 0 \\ 0 & 0 & 0 & 0 & 0 & -\frac{1}{c} & 0 & \frac{1}{c}+c & -c & 0 \\ 0 & 0 & 0 & 0 & -\frac{1}{2c} & 0 & 0 & -2+c & 2+\frac{1}{c^2}-c & -\frac{1}{c^2}+\frac{1}{2c} \\ 0 & 0 & 0 & 0 & 0 & 0 & 0 & 0 & -\frac{1}{2c} & -1 \end{pmatrix}$$

$$B3 = \begin{pmatrix} b11 \\ b21 \\ b31 \\ b41 \\ b51 \\ b61 \\ b71 \\ b81 \\ b91 \\ b101 \end{pmatrix} \qquad B4 = \begin{pmatrix} d11 \\ d21 \\ d31 \\ d41 \\ d51 \\ d61 \\ d71 \\ d81 \\ d91 \\ d101 \end{pmatrix}$$

$$B5 = \begin{pmatrix} -\frac{1}{18}c\left(-dG\theta_2 - dG\theta_7\right) \\ \frac{dRN_7}{2c} - \frac{1}{18}c\left(-4dG\theta_2 + 2dG\theta_3 - dG\theta_6\right) + \frac{18dRN_7 - 9cdRN_7 + 3cdG\theta_2 - 9c^2dG\theta_2 + 4c^3dG\theta_2 - 3cdG\theta_7 + c^3dG\theta_7}{18c^2} \\ \frac{dRN_6}{2c} - \frac{1}{18}c\left(4dG - 7dG\theta_3\right) + \frac{18dRN_6 - 9cdRN_6 - 3c^2dG\theta_2 + c^3dG\theta_2 + 3cdG\theta_3 - 3c^2dG\theta_3 + c^3dG\theta_3 - 3cdG\theta_6 + c^3dG\theta_6}{18c^2} \\ \frac{3c^2dG - c^3dG - 9c^2dG\theta_3 + 4c^3dG\theta_3}{18c^2} \\ -\frac{-3cdG + c^2dG + 9(-2+c)cdRN_6 - 3dG\theta_3 + 6cdG\theta_3 - 2c^2dG\theta_3 + 3dG\theta_6 + 3cdG\theta_6 - 2c^2dG\theta_6}{18c} - \frac{3c^2dG - 2c^3dG + 9(-2+c)c^2dRN_6 + 3c^2dG\theta_6 - c^3dG\theta_6}{18c^2} \\ c61 \\ -\frac{dRN_7}{2c} - \frac{-9c^2dRN_6 + 9dRN_7 + 9c^2dRN_7 - 2c^2dG\theta_2 - 2c^2dG\theta_6 + c^2dG\theta_7}{18c} - \frac{1}{18}c\left(-9dRN_6 + 9dRN_7 + 2dG\theta_6 - 7dG\theta_7 + 2dG\theta_8\right) \\ -\frac{-dRN_6 + dRN_8}{2c} - \frac{1}{18}c\left(4dG + 9dRN_8 - 7dG\theta_8\right) - \frac{c^2dG - 9dRN_6 + 9dRN_8 + 9c^2dRN_8 - 5c^2dG\theta_8 + c^2dG\theta_8}{18c} \\ -\frac{-3cdG + c^2dG + 9(-2+c)cdRN_8 - 3dG\theta_6 + 12cdG\theta_6 - 5c^2dG\theta_6 + 3dG\theta_8 - 3cdG\theta_8 + c^2dG\theta_8}{18c} - \frac{-3c^2dG + c^3dG + 9(-2+c)c^2dRN_8 + 9c^2dG\theta_8 - 4c^3dG\theta_8}{18c^2} \\ 0 \end{pmatrix}$$

The domain consists three horizontal levels and the solution for Ψ, θ and N at each level may be expressed in terms of the nodal values as follows,

In the horizontal strip $0 \le y \le \frac{h}{3}$

$\Psi = (\Psi_1 N^1_1 + \Psi_2 N^1_2 + \Psi_7 N^1_7)\, H(1-\tau_1)$

$= \Psi_1 (1-4x) + \Psi_2 4(x-\frac{y}{h}) + \Psi_7 (\frac{4y}{h})\, (1-\tau_1)$ $\quad (0 \le x \le \frac{1}{3})$

$\Psi = (\Psi_2 N^3_2 + \Psi_3 N^3_3 + \Psi_6 N^3_6)\, H(1-\tau_2)$

$+ (\Psi_2 N^2_2 + \Psi_7 N^2_7 + \Psi_6 N^2_6) H(1-\tau_3)$ $\quad (\frac{1}{3} \le x \le \frac{1}{3})$

$= (\Psi_2 2(1-2x) + \Psi_3 (4x-\frac{4y}{h} -1) + \Psi_6 (\frac{4y}{h}))H(1-\tau_2)$

$+ (\Psi_2 (1-\frac{4y}{h}) + \Psi_7 (1+\frac{4y}{h} -4x) + \Psi_6 (4x-1))H(1-\tau_3)$

$\Psi = (\Psi_3 N^5_3 + \Psi_4 N^5_4 + \Psi_5 N^5_5)\, H(1-\tau_3)$

$+ (\Psi_3 N^4_3 + \Psi_5 N^4_5 + \Psi_6 N^4_6) H(1-\tau_4)$ $\quad (\frac{2}{3} \le x \le 1)$

$= (\Psi_3 (3-4x) + \Psi_4 2(2x-\frac{2y}{h} -1) + \Psi_6 (\frac{4y}{h} -4x+3))H(1-\tau_3)$

$+ \Psi_3 (1-\frac{4y}{h}) + \Psi_5 (4x-3) + \Psi_6 (\frac{4y}{h}))H(1-\tau_4)$

Along the strip $\frac{h}{3} \le y \le \frac{2h}{3}$

$\Psi = (\Psi_7 N^6_7 + \Psi_6 N^6_6 + \Psi_8 N^6_8)\, H(1-\tau_2)$ $\quad (\frac{1}{3} \le x \le 1)$

$+ (\Psi_6 N^7_6 + \Psi_9 N^7_9 + \Psi_8 N^7_8)\, H(1-\tau_3) + (\Psi_6 N^8_6 + \Psi_5 N^8_5 + \Psi_9 N^8_9)\, H(1-\tau_4)$

$\Psi = (\Psi_7 2(1-2x) + \Psi_6 (4x-3) + \Psi_8 (\frac{4y}{h} -1))H(1-\tau_3)$

$+ \Psi_6 (2(1-\frac{2y}{h}) + \Psi_9 (\frac{4y}{h} -1) + \Psi_8 (1+\frac{4y}{c} -4x))H(1-\tau_4)$

$+ \Psi_6 (4(1-x) + \Psi_5 (4x-\frac{4y}{c} -1) + \Psi_9 2(\frac{2y}{h} -1))H(1-\tau_5)$

Along the strip $\frac{2h}{3} \le y \le 1$

$\Psi = (\Psi_8 N^9_8 + \Psi_9 N^9_9 + \Psi_{10} N^9_{10})\, H(1-\tau_6)$ $\quad (\frac{2}{3} \le x \le 1)$

$= \Psi_8 (4(1-x) + \Psi_9 4(x-\frac{y}{h}) + \Psi_{10} 2(\frac{4y}{h} -3))H(1-\tau_6)$

where $\tau_1 = 4x$, $\tau_2 = 2x$, $\tau_3 = \frac{4x}{3}$,

$\tau_4 = 4(x-\frac{y}{h})$, $\tau_5 = 2(x-\frac{y}{h})$, $\tau_6 = \frac{4}{3}(x-\frac{y}{h})$

And H represents the Heaviside function.
The expressions for θ are

In the horizontal strip $0 \le y \le \frac{h}{3}$

$\theta = [\theta_1 (1-4x) + \theta_2 4(x-\frac{y}{h}) + \theta_7 (\frac{4y}{h})) H (1-\tau_1)$ $(0 \le x \le \frac{1}{3})$

$\theta = (\theta_2(2(1-2x) + \theta_3 (4x-\frac{4y}{c} -1) + \theta_6(\frac{4y}{c})) H (1-\tau_2)$

$+ \theta_2(1-\frac{4y}{h}) + \theta_7(1+\frac{4y}{h} -4x) + \theta_6(4x-1)) H (1-\tau_3)$ $(\frac{1}{3} \le x \le \frac{2}{3})$

$\theta = \theta_3(3-4x) +2 \theta_4(2x-\frac{2y}{h} -1) + \theta_6(\frac{4y}{h} -4x+3) H (1-\tau_3)$

$+ (\theta_3(1-\frac{4y}{h}) + \theta_5(4x-3) + \theta_6(\frac{4y}{h})) H (1-\tau_4)$ $(\frac{2}{3} \le x \le 1)$

Along the strip $\frac{h}{3} \le y \le \frac{2h}{3}$

$\theta = (\theta_7(2(1-2x) + \theta_6(4x-3) + \theta_8(\frac{4y}{h} -1)) H (1-\tau_3)$ $(\frac{1}{3} \le x \le \frac{2}{3})$

$+ (\theta_6(2(1-\frac{2y}{h}) + \theta_9(\frac{4y}{h} -1) + \theta_8(1+\frac{4y}{h} -4x)) H (1-\tau_4)$

$+ (\theta_6(4(1-x) + \theta_5(4x-\frac{4y}{h} -1) + \theta_9 2(\frac{4y}{h} -1)) H (1-\tau_5)$

Along the strip $\frac{2h}{3} \le y \le 1$

$\theta = (\theta_8 4(1-x) + \theta_9 4(x-\frac{y}{h}) + \theta_{10}(\frac{4y}{h} -3) H(1-\tau_6)$ $(\frac{2}{3} \le x \le 1)$

The expressions for N are

$N = [N_1(1-4x) + N_2 4(x-\frac{y}{c}) + N_7 (\frac{4y}{c})) H(1-\tau_1)$ $(0 \le x \le \frac{1}{3})$

$N = (N_2(2(1-2x) + N_3 (4x-\frac{4y}{h} -1) + N_6(\frac{4y}{h})) H(1-\tau_2)$

$+ N_2(1-\frac{4y}{h}) + N_7(1+\frac{4y}{h} -4x) + N_6(4x-1)) H(1-\tau_3)$ $(\frac{1}{3} \le x \le \frac{2}{3})$

$N = N_3(3-4x) +2 N_4(2x-\frac{2y}{h} -1) + N_6(\frac{4y}{h} -4x+3) H(1-\tau_3)$

$+ (N_3(1-\frac{4y}{h}) + N_5(4x-3) + N_6(\frac{4y}{h})) H(1-\tau_4)$ $(\frac{2}{3} \le x \le 1)$

Along the strip $\frac{h}{3} \le y \le \frac{2h}{3}$

$N = (N_7(2(1-2x) + N_6(4x-3) + N_8(\frac{4y}{c} -1)) H(1-\tau_3)$ $(\frac{1}{3} \le x \le \frac{2}{3})$

$+ (N_6(2(1-\frac{2y}{h}) + N_9(\frac{4y}{h} -1) + N_8(1+\frac{4y}{h} -4x)) H(1-\tau_4)$

$+ (N_6(4(1-x) + N_5(4x-\frac{4y}{h} -1) + N_9 2(\frac{4y}{h} -1)) H(1-\tau_5)$

Along the strip $\frac{2h}{3} \le y \le 1$

$N = (N_8 4\,(1-x) + N_9 4(x - \frac{y}{h}) + N_{10}\,(\frac{4y}{h} - 3)\,H(1-\tau_6)$ $\quad (\frac{2}{3} \le x \le 1)$

The dimensionless Nusselt numbers on the non-insulated boundary walls of the rectangular duct are calculated using the formula

$$N_u = (\frac{\partial \theta}{\partial x})_{x=1}$$

Nusselt number on the side wall x=1 in the different regions are

$Nu_1 = 2 - 4\,\theta_3$, $\quad M_1^* = 2 - 4N_3$ $\quad 0 \le y \le \frac{c}{3}$

$Nu_2 = 2 - 4\,\theta_6$ $\quad M_2^* = 2 - 4N_6$ $\quad \frac{c}{3} \le y \le 2\frac{c}{3}$

$Nu_3 = 2 - 4\,\theta_9$, $\quad M_3^* = 2 - 4N_9$ $\quad \frac{2c}{3} \le y \le 1$

The details of a_{11}, b_{11}, a_{r1}, b_{r1}, c_{r1} etc., are shown in appendix

The equilibrium conditions are

$$R_3^1 + R_1^2 = 0, \quad R_3^2 + R_1^3 = 0$$
$$R_3^3 + R_1^4 = 0, \quad R_3^4 + R_1^5 = 0$$
$$Q_3^1 + Q_1^2 = 0, \quad Q_3^2 + Q_1^3 = 0$$
$$Q_3^3 + Q_1^4 = 0, \quad Q_3^4 + Q_1^5 = 0$$
$$S_3^1 + S_1^2 = 0, \quad S_3^2 + S_1^3 = 0$$
$$S_3^3 + S_1^4 = 0, \quad S_3^4 + S_1^5 = 0 \qquad 4.4$$

Solving these coupled global matrices for temperature, Micro concentration and velocity (4.1 – 4.3) respectively and using the iteration procedure we determine the unknown global nodes through which the temperature, Micro rotation and velocity of different intervals at any arbitrary axial cross section are obtained.

V. DISCUSSION

In this analysis we investigate the effect of dissipation and heat sources on convective heat and mass transfer flow of a micropolar fluid through a porous medium in a rectangular duct. The non-linear coupled equations governing the flow, heat and mass transfer have been solved by using Galerikin finite element analysis with three nodded triangular elements and Prandtl number Pr is taken as 0.71.

The non-dimensional temperature 'θ' is exhibited in fig 1-12 for different values of G, D^{-1}, Sc, N,α, Ec, R & λ at different levels. We follow the convention that, the non-dimensional temperature is positive or negative according as the actual temperature is greater/smaller than the equilibrium temperature.

Figs. (1-4) represent θ with G, D^{-1} & Sc. It is found that an increase in G enhances the actual temperature at $y = \frac{2h}{3}$ level, $x = \frac{1}{3}$ & $x = \frac{2}{3}$ levels and reduces at $y = \frac{h}{3}$ level. With respect to Darcy parameter D^{-1}, we find the lesser the permeability of the porous medium larger the actual temperature at $y = \frac{2h}{3}$, $x = \frac{1}{3}$ & $x = \frac{2}{3}$ levels and smaller at $y = \frac{h}{3}$ level. The variation of θ with Schmidt number Sc shows that lesser the molecular diffusivity larger the actual temperature at $y = \frac{2h}{3}$ and $y = \frac{h}{3}$ levels and smaller at $x = \frac{1}{3}$ level.

At x=2/3

level an increase in Sc ≤ 0.6 enhances the actual temperature while it reduces with higher Sc ≥ 1.3 (figs 1-4).Figs (5-8) represent 'θ' with N & α at different levels. It is found that when the molecular buoyancy force dominates over the thermal buoyancy force, the actual temperature enhances at $y=\frac{2h}{3}$, $x=\frac{1}{3}$ and $x=\frac{2}{3}$ levels and reduces at $y=\frac{h}{3}$ level when the buoyancy forces are in the same direction and for the forces acting in the opposite directions, the actual temperature reduces at $y=\frac{2h}{3}, y=\frac{h}{3}$, $x=\frac{1}{3}$ levels and at $x=\frac{2}{3}$ level, it enhances in the horizontal region (0 ≤ y ≤ 0.264) and reduces in the region (0.333 ≤ y ≤ 0.666).The variation of θ with heat source parameter 'α' shows that at $y=\frac{2h}{3}$ level, the actual temperature reduces with α > 0 and enhances |α|. At $y=\frac{h}{3}$ level, the actual temperature reduces for α ≤ 4 and enhances at higher α > 6 while it reduces |α| (fig. 5). At $x=\frac{1}{3}$ level, the temperature enhances in the region (0, 0.067) and reduces in the region (0.134, 0.333) for α ≤ 4. For higher α ≥ 6 the actual temperature reduces in the region (0, 0.201) and enhances in the region (0.268, 0.333). An increase in |α| leads to a depreciation in the actual temperature (fig. 7). At $x=\frac{2}{3}$ level, an increase in α ≤ 4 reduces the actual temperature except in the horizontal strip (0, 0.066) and for higher α ≥ 6, the actual temperature increase in the region (0, 0.333) and reduces in the region (0.369, 0.666). An increase in |α| results in an enhancement in the actual temperature (fig. 8).Figs (9-12) represent θ with Ec, R &λ. It is found that higher the dissipative heat larger the actual temperature at $y=\frac{h}{3}$ and $x=\frac{1}{3}$ levels and smaller at $y=\frac{2h}{3}$ and $x=\frac{2}{3}$ levels. An increase in micro rotation parameter R reduces the actual temperature at $y=\frac{2h}{3}$, $y=\frac{h}{3}$ and $x=\frac{1}{3}$ levels. At $x=\frac{2}{3}$ level the actual temperature enhances in the horizontal strip (0, 0.132) and reduces in the region (0.198, 0.666). An increase in the spin gradient parameter λ leads to an enhancement in the actual temperature at all levels (figs 9-12).

The non-dimensional concentration (C) is shown in figs 13-24 for different parametric values. We follow the convention that the concentration is positive or negative according as the actual concentration is greater/lesser than the equilibrium concentration. Figs (13-16) represent the concentration. 'C' with G, D^{-1} & Sc. It is found that the actual concentration enhances at $y=\frac{2h}{3}$ and $x=\frac{1}{3}$ levels, while it reduces at $y=\frac{h}{3}$ and $x=\frac{2}{3}$ level. With reference to D^{-1} we find that lesser the permeability of the porous medium, larger the actual concentration at $y=\frac{2h}{3}$ and $x=\frac{1}{3}$ levels and smaller at $y=\frac{h}{3}$ level. At $x=\frac{2}{3}$ level the concentration reduces with D^{-1} in the horizontal strip (0, 0.333) and enhances in the region (0.369, 0.666). With reference to Sc, we find that lesser the molecular diffusivity smaller the actual concentration at both the horizontal levels. At $x=\frac{1}{3}$ level the actual concentration enhances with Sc ≤ 0.6 in the region (0, 0.134) and reduces in the region (0.201, 0.333) and for higher Sc ≥ 1.3, we notice a depreciation everywhere in the region except in the region (0, 0.666) (figs 13-16).

Figs (17- 20) represent concentration with buoyancy ratio 'N' and heat source parameter α. It is found that the molecular buoyancy force dominates over the thermal buoyancy force, the actual concentration reduces at both the horizontal levels and enhances at both the vertical level when the buoyancy forces are in the same direction and for the forces acting in opposite directions, the actual concentration reduces at all levels. With reference to heat source parameter α, we find that the actual concentration reduces with increase in α ≤ 4 and enhances with

higher $\alpha \geq 6$. An increase in the strength of heat absorbing source $|\alpha|(<0)$ enhances the actual concentration at both the horizontal levels. At $x = \frac{1}{3}$ level, the actual concentration enhances in the region (0, 0.134) and reduces in the region (0.201, 0.333) with $\alpha \leq 4$ and for higher $\alpha \geq 6$; we notice an enhancement in the actual concentration. At $x = \frac{2}{3}$ level the actual concentration reduces with $|\alpha|$ in the region (0, 0.132) and enhances in the region (0.201, 0.666) (figs 17-20).

Figs (21-24) represents the concentration with Ec, R andλ. It is found that higher the dissipative heat smaller the actual concentration at both the horizontal levels and larger at $x = \frac{1}{3}$ level. At $x = \frac{2}{3}$ level, higher the dissipative heat larger the actual concentration in the region (0, 0.264) and smaller in the region (0.333, 0.666). An increase in R enhances the actual concentration at all levels. An increase in spin gradient parameter λ leads to the depreciation at both the horizontal levels and at $x = \frac{2}{3}$ level, while it enhances at $x = \frac{1}{3}$ level. (Figs 21-24).

Figs 25-28 represent micro rotation (ω)with different value of G, D^{-1} & Sc. It is found that at $y = \frac{h}{3}$, $x = \frac{1}{3}$ & $x = \frac{2}{3}$ levels, the micro-rotation enhances with increasing $G \leq 2\times10^2$ and reduces for $G \geq 3\times10^2$ while at $y = \frac{2h}{3}$ level, the micro rotation enhances with G. With respect to D^{-1}, we find that the micro rotation reduces with $D^{-1} \leq 10$ and enhances with $D^{-1} \geq 15$ at $y = \frac{h}{3}$, $x = \frac{1}{3}$ & $x = \frac{2}{3}$ levels, while it enhances with D^{-1}, at $y = \frac{2h}{3}$ level, The variation on ω with Schmidt number Sc shows that lesser the molecular diffusivity smaller the micro rotation at $y = \frac{h}{3}$ & $x = \frac{1}{3}$ levels. At $y = \frac{2h}{3}$ level the micro-rotation reduces with $Sc \leq 0.6$ and enhances with higher $Sc \geq 1.3$. At $x = \frac{2}{3}$ level, the micro rotation enhances with $Sc \leq 0.6$ and for higher Sc = 1.3, it reduces and for still higher $Sc \geq 2.01$ we notice an enhancement in the micro-rotation. (Figs 25-28). Figs.29-32 represents micro rotation with buoyancy ratio N and heat source parameterα. It is found that when the molecular buoyancy force dominates over the thermal buoyancy force, the micro rotation reduces at $y = \frac{h}{3}$ & $x = \frac{1}{3}$ levels and enhances at $y = \frac{2h}{3}$ level irrespective of the directions of the buoyancy forces. At $x = \frac{2}{3}$ levels, the micro rotation enhances with $N > 0$ and reduces with $|N|$. With respect to heat source parameter α we find that the micro rotation reduces at $y = \frac{h}{3}$ & $x = \frac{1}{3}$ level. At $y = \frac{2h}{3}$ and $x = \frac{2}{3}$ levels, the micro rotation enhances with $\alpha \leq 4$ and reduces with higher $\alpha \geq 6$ while it reduces with the strength of the heat absorption source $|\alpha|$ (figs 29-32). With respect to Ec we find that higher the dissipative heat larger the micro rotation at all levels. An increase in the micro rotation parameter 'R' enhances the micro rotation at all levels. With respect to spin gradient parameterλ, we find that the micro rotation enhances at $y = \frac{2h}{3}$ and $x = \frac{1}{3}$ levels and reduces at $y = \frac{2h}{3}$ & $x = \frac{2}{3}$ levels (figs 33-36).

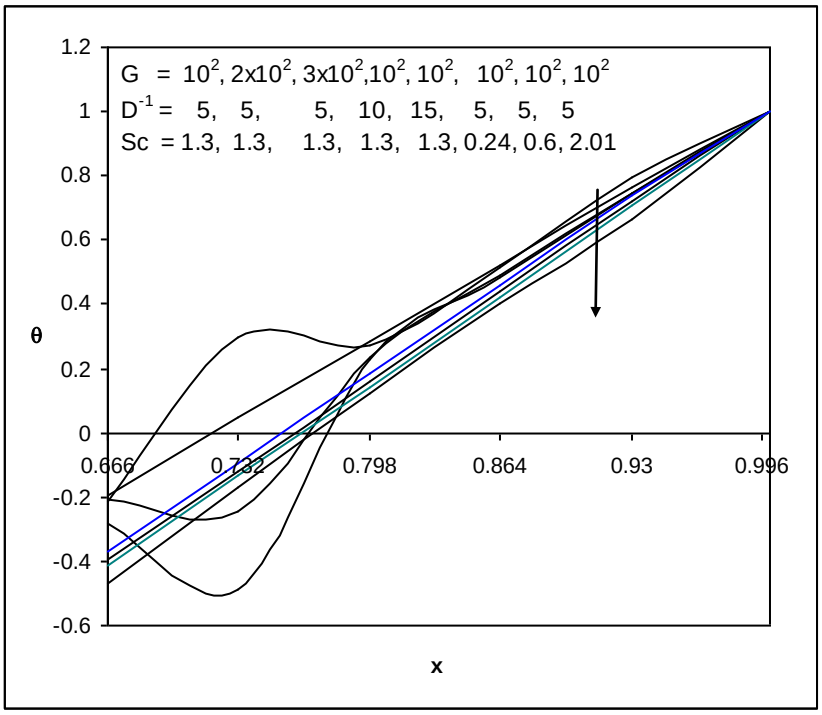

Fig. 1: Variation of θ with G, D^{-1}, Sc at $y = \frac{2h}{3}$ level

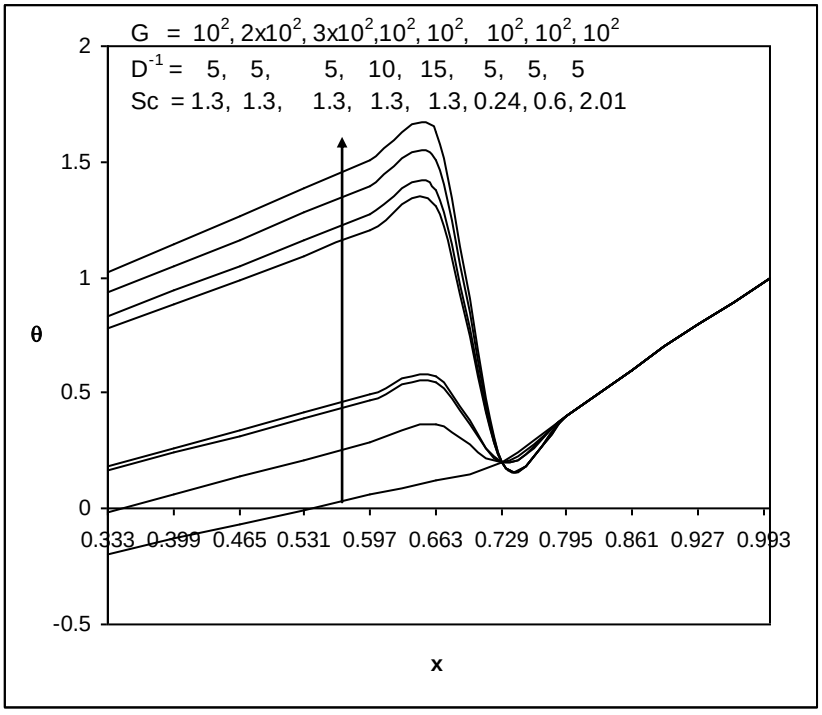

Fig. 2: Variation of θ with G, D^{-1}, Sc at $y = \frac{h}{3}$ level

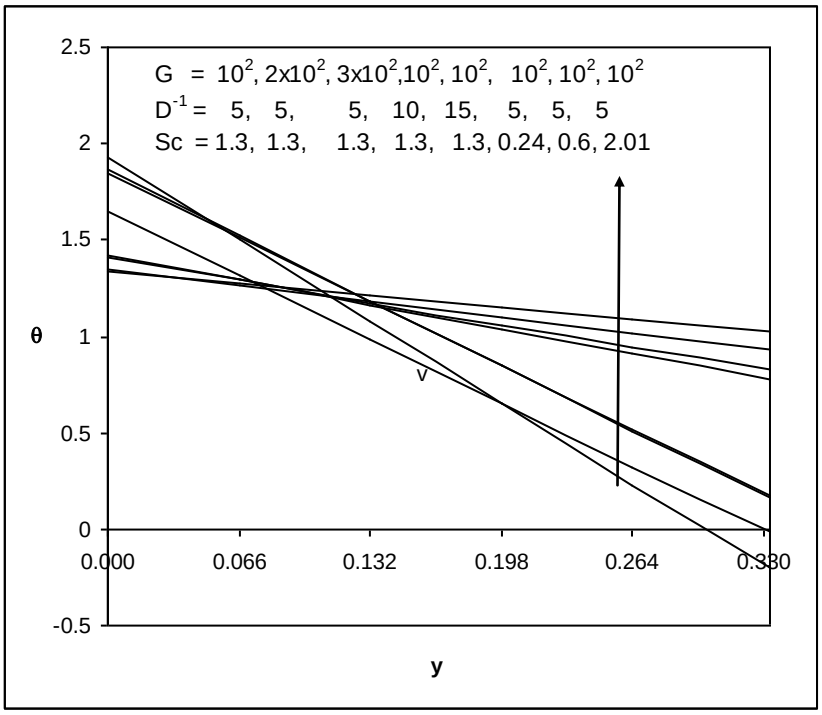

Fig. 3: Variation of θ with G, D^{-1}, Sc at $x = \frac{1}{3}$ level

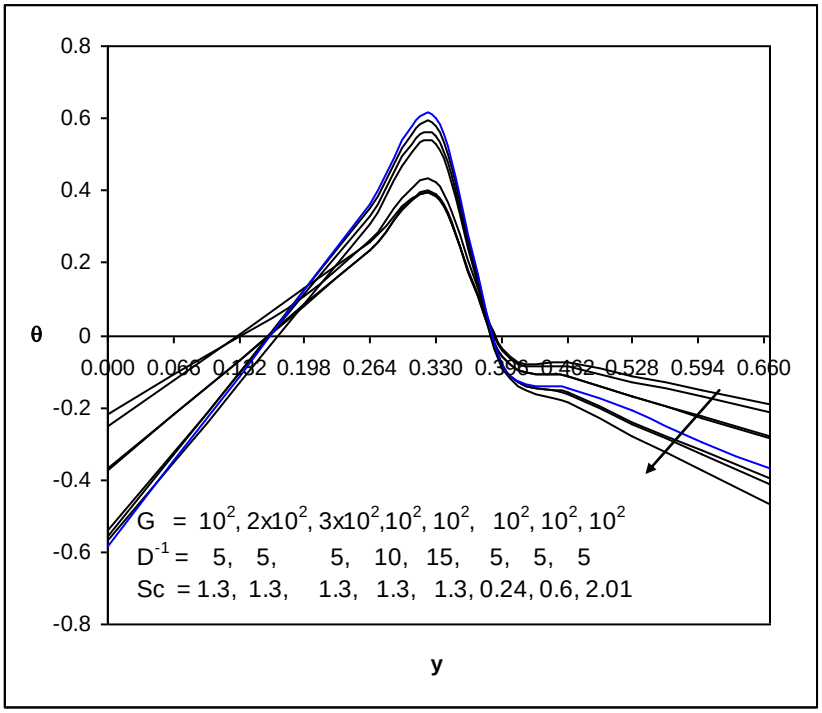

Fig. 4: Variation of θ with G, D^{-1}, Sc at $x = \frac{2}{3}$ level

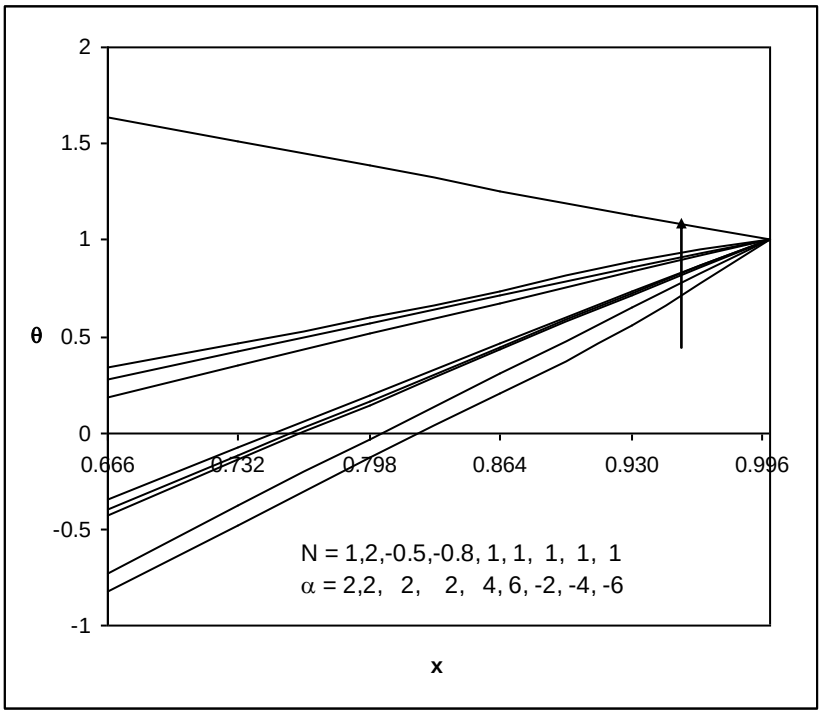

Fig. 5: Variation of θ with N, α at $y = \frac{2h}{3}$ level

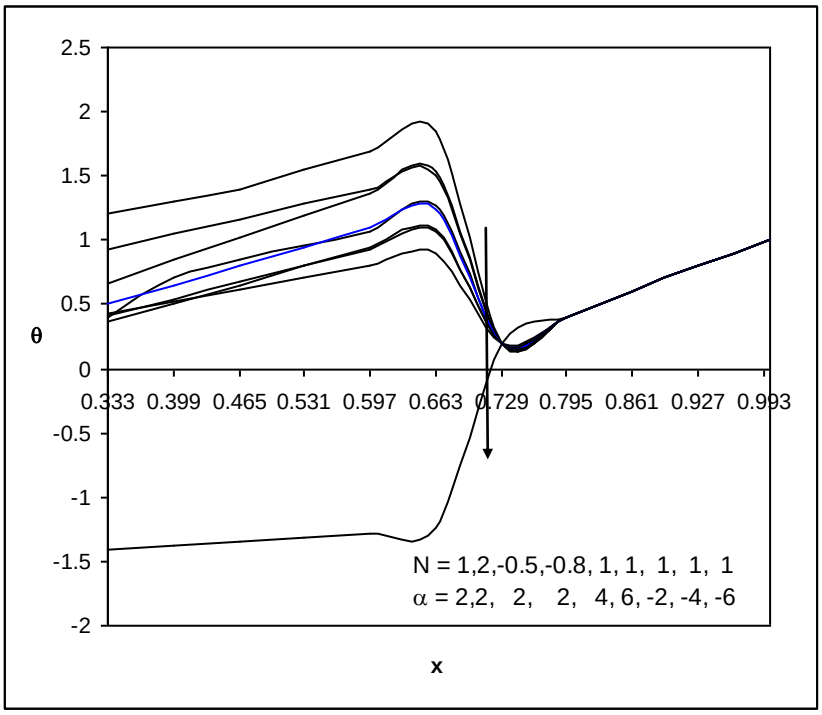

Fig. 6: Variation of θ with N, α at $y = \frac{h}{3}$ level

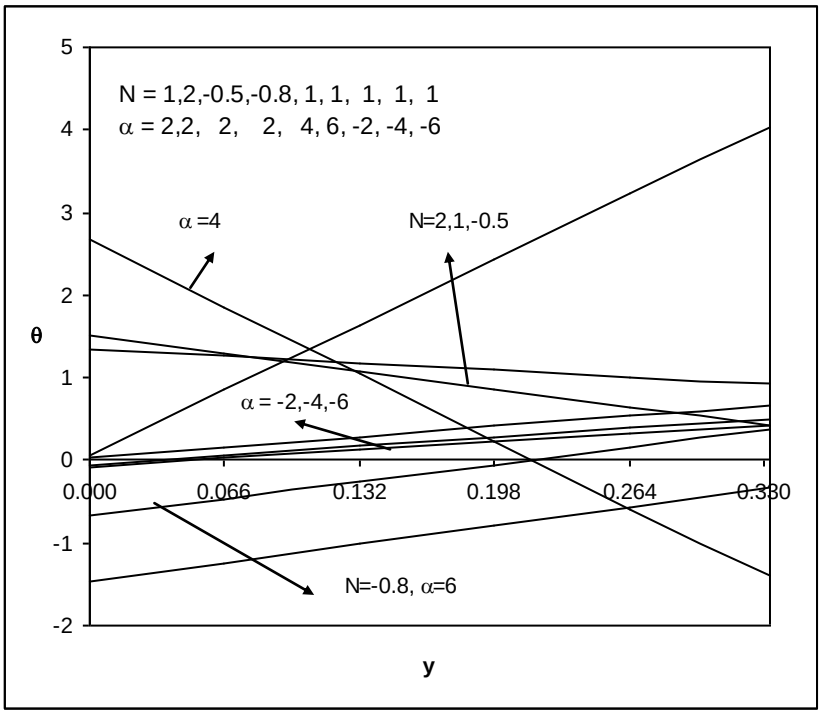

Fig. 7: Variation of θ with N, α at $x = \frac{1}{3}$ level

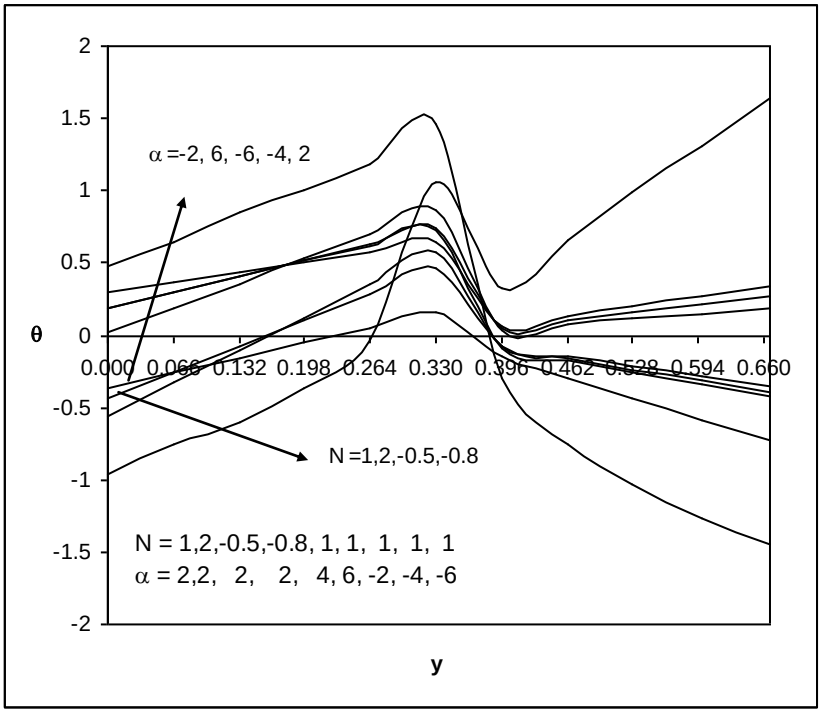

Fig. 8: Variation of θ with N, α at $x = \frac{2}{3}$ level

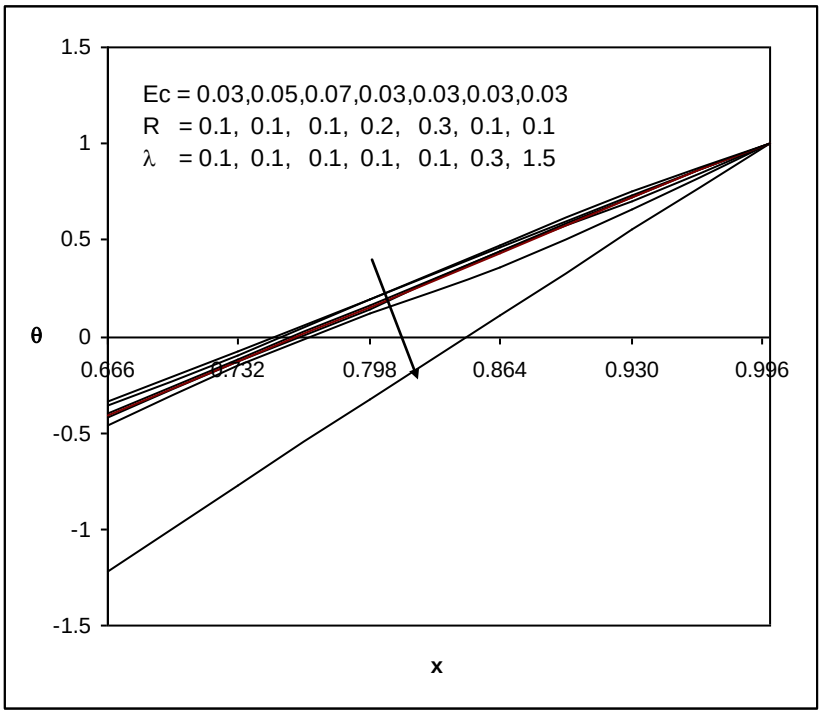

Fig. 9: Variation of θ with Ec, R, λ at $y = \frac{2h}{3}$ level

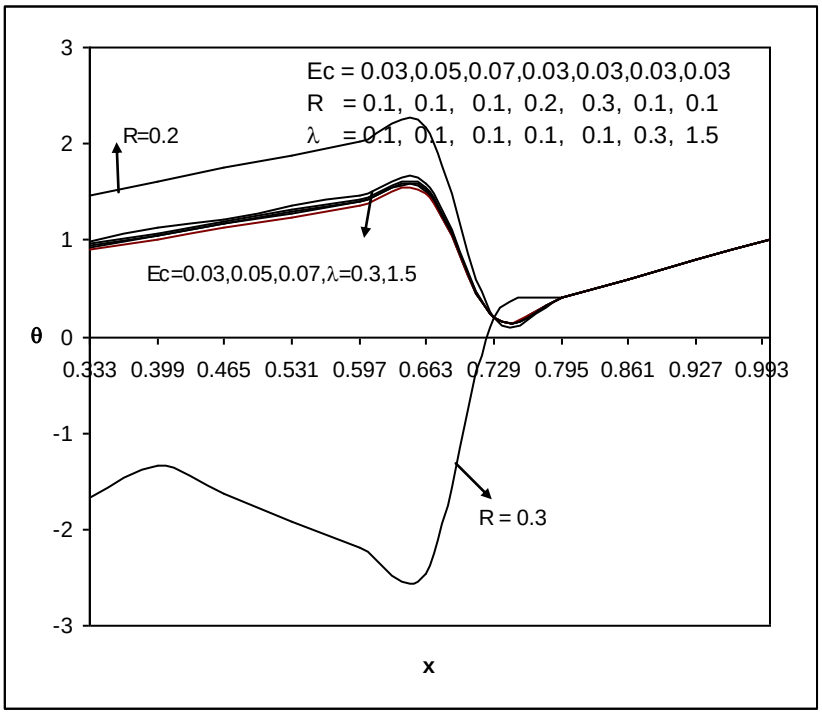

Fig. 10: Variation of θ with Ec, R, λ at $y = \frac{h}{3}$ level

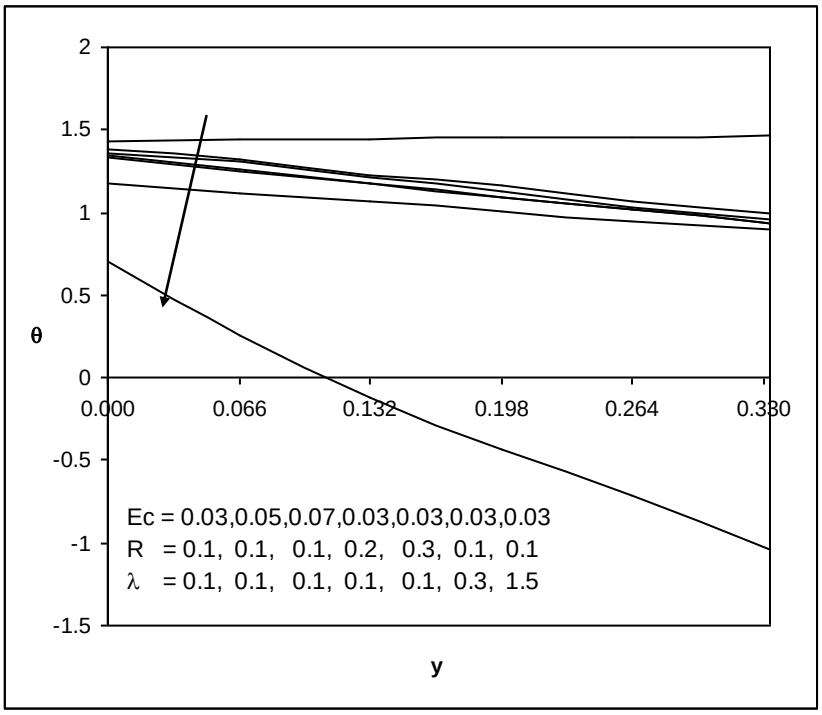

Fig. 11: Variation of θ with Ec, R, λ at $x = \frac{1}{3}$ level

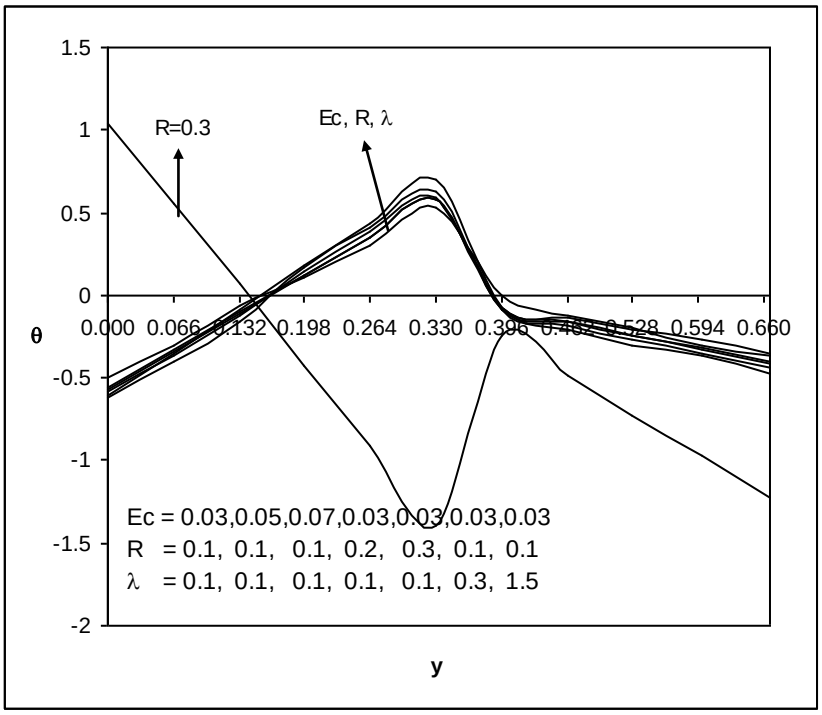

Fig. 12: Variation of θ with Ec, R, λ at $x = \frac{2}{3}$ level

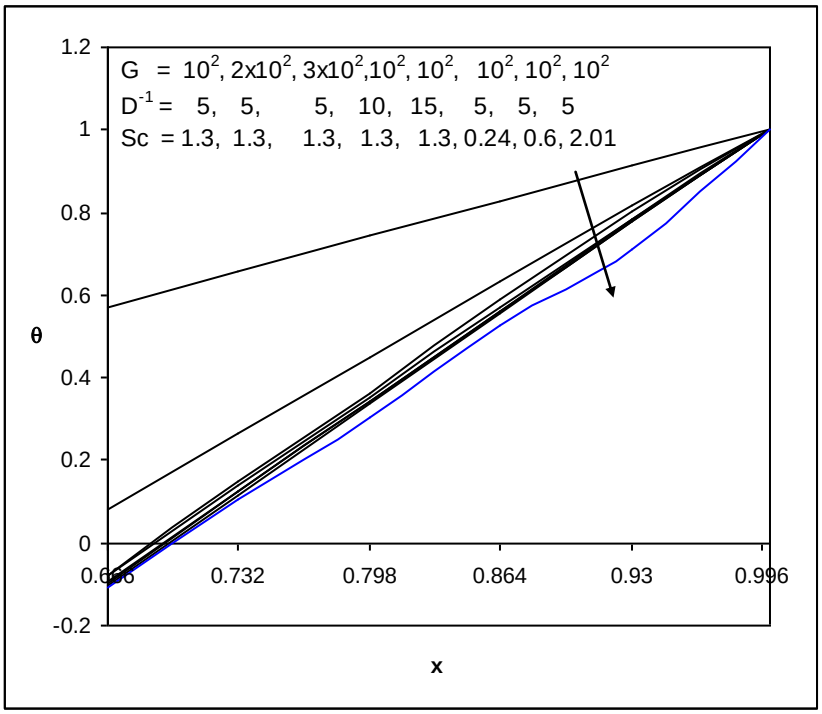

Fig. 13: Variation of C with G, D^{-1}, Sc at $y = \frac{2h}{3}$ level

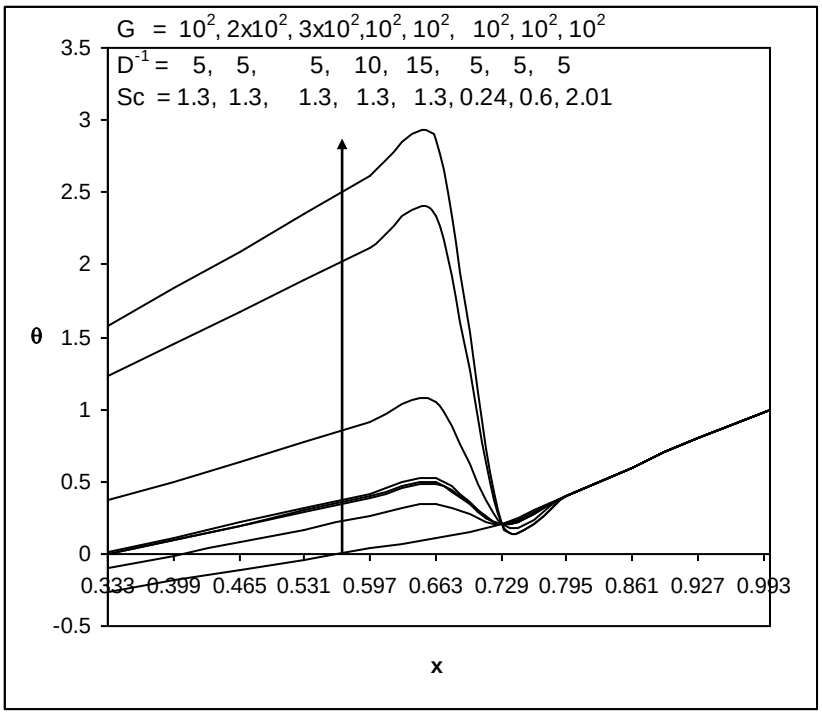

Fig. 14: Variation of C with G, D^{-1}, Sc at $y = \frac{h}{3}$ level

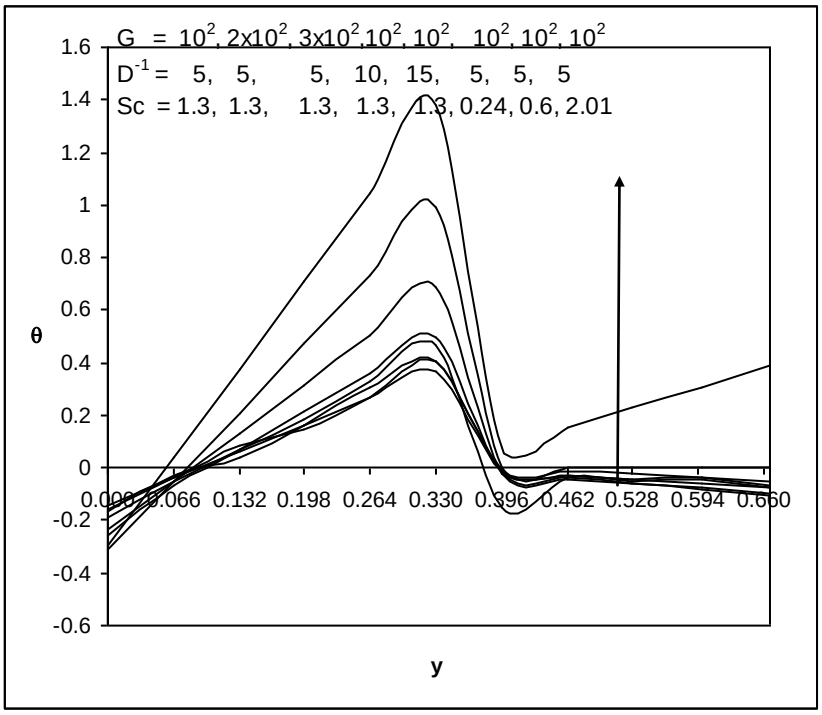

Fig. 15: Variation of C with G, D^{-1}, Sc at $x = \frac{1}{3}$ level

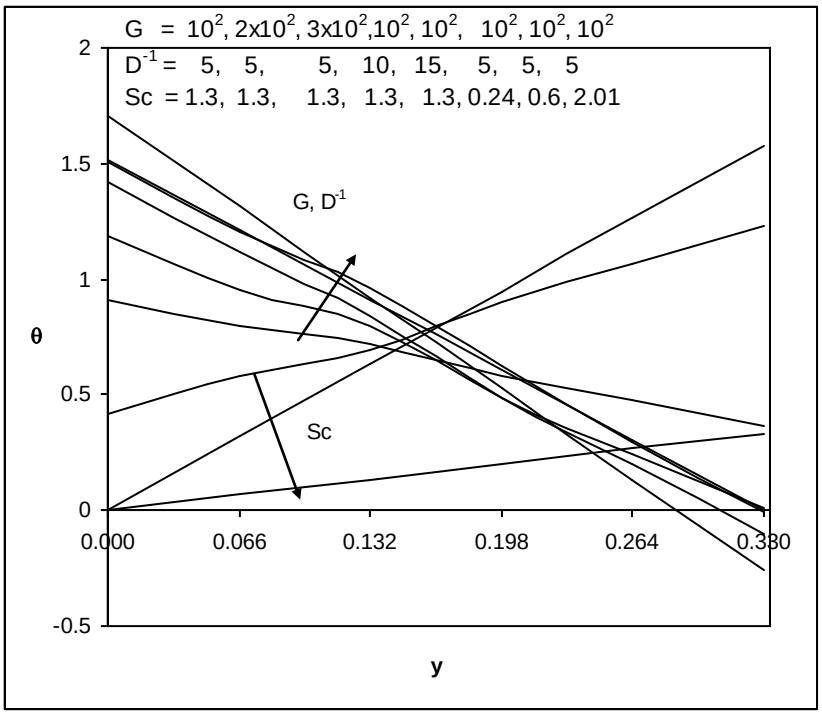

Fig. 16: Variation of C with G, D^{-1}, Sc at $x = \frac{2}{3}$ level

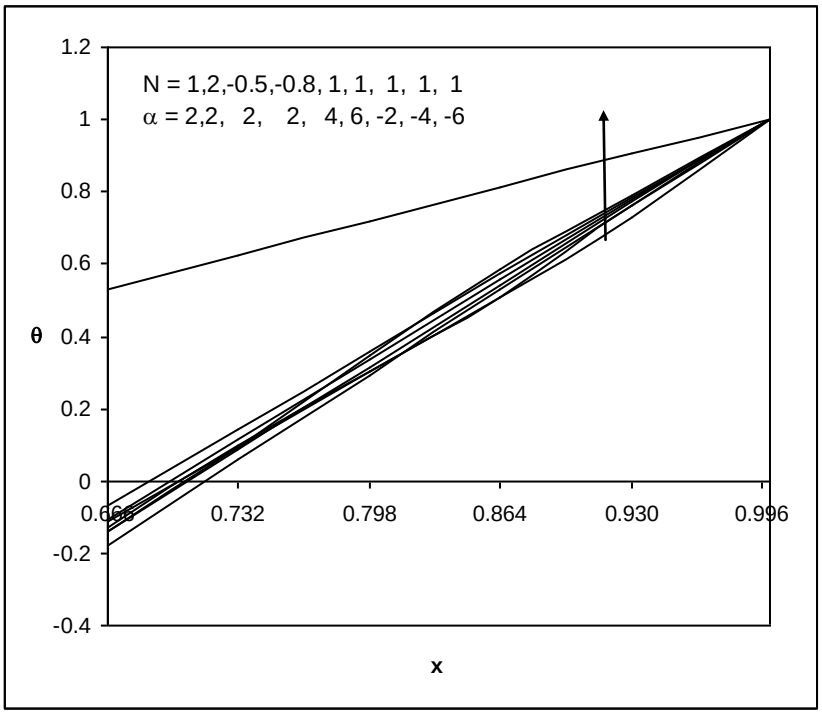

Fig. 17: Variation of C with N, α at $y = \frac{2h}{3}$ level

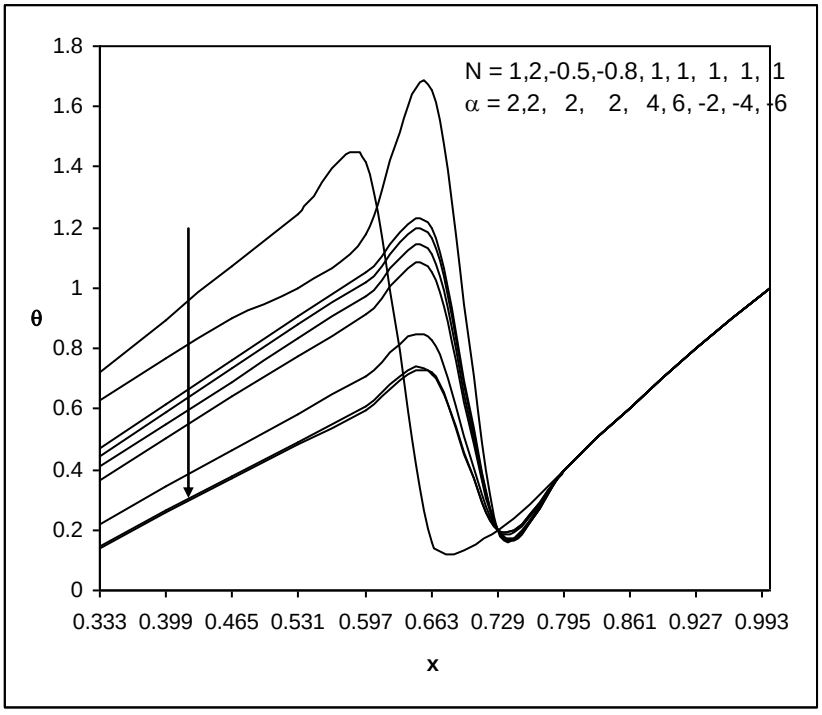

Fig. 18: Variation of C with N, α at $y = \frac{h}{3}$ level

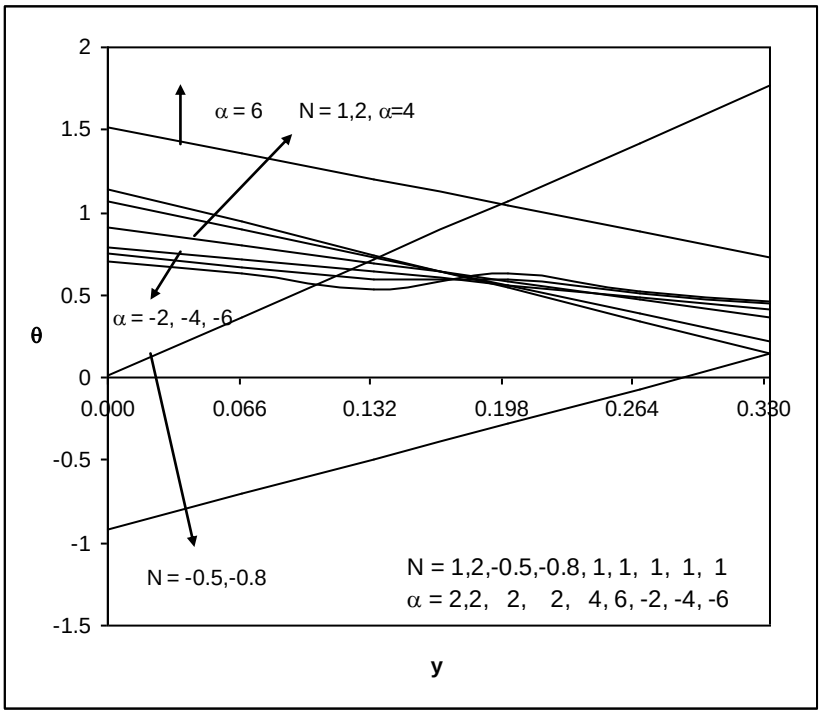

Fig. 19: Variation of C with N, α at $x = \frac{1}{3}$ level

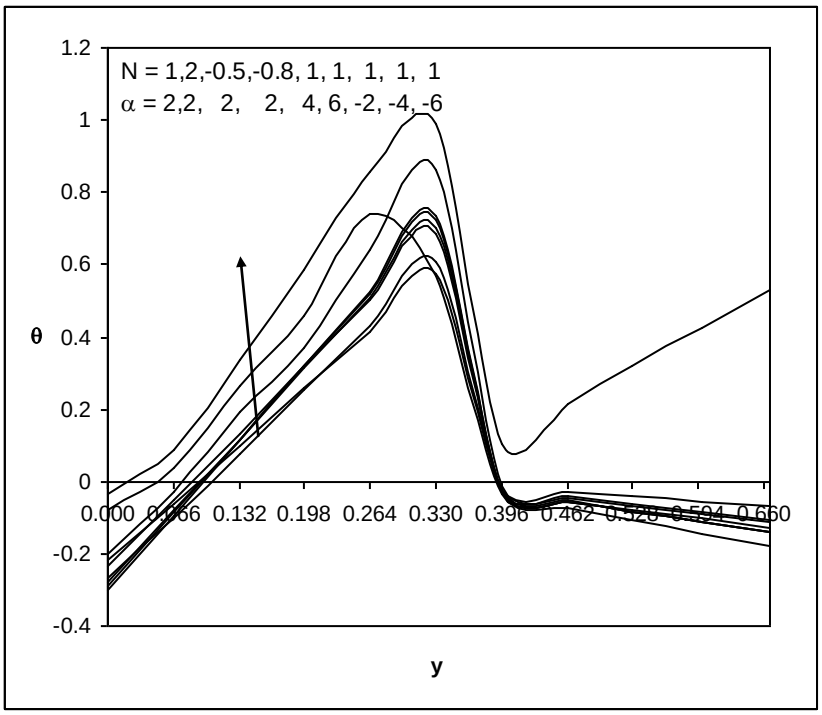

Fig. 20: Variation of C with N, α at $x = \frac{2}{3}$ level

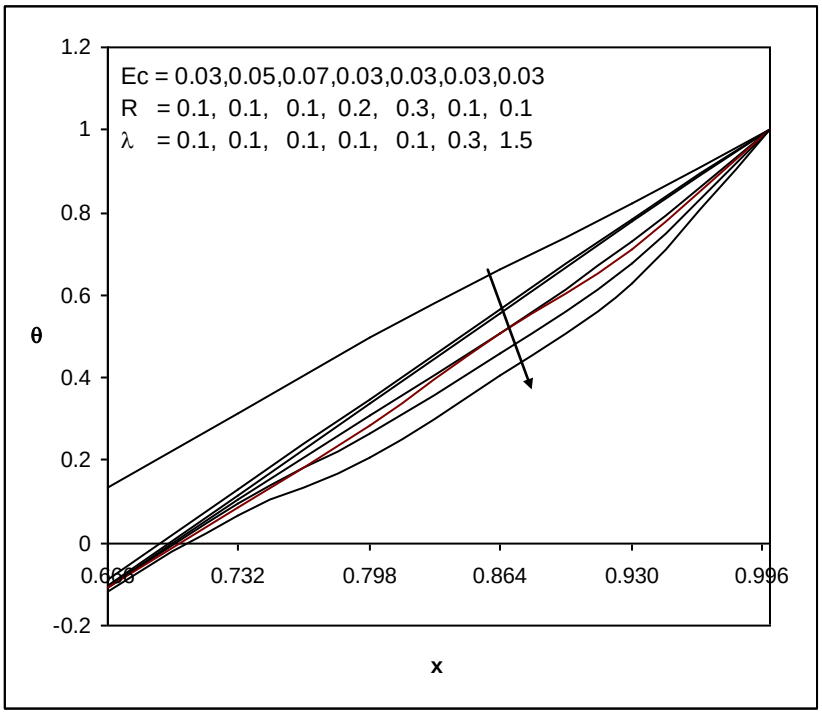

Fig. 21: Variation of C with Ec, R, λ at $y = \frac{2h}{3}$ level

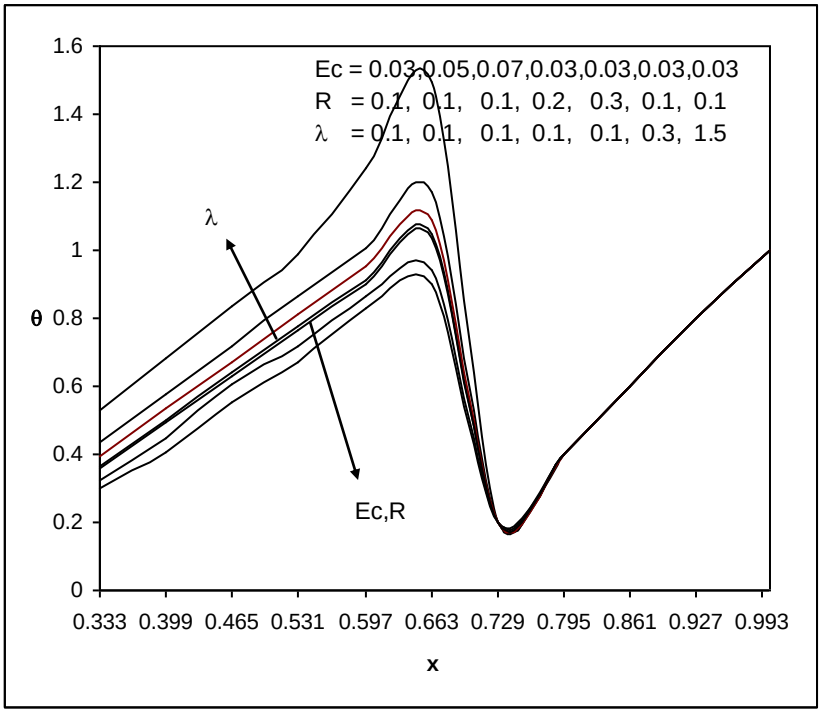

Fig. 22: Variation of C with Ec, R, λ at $y = \frac{h}{3}$ level

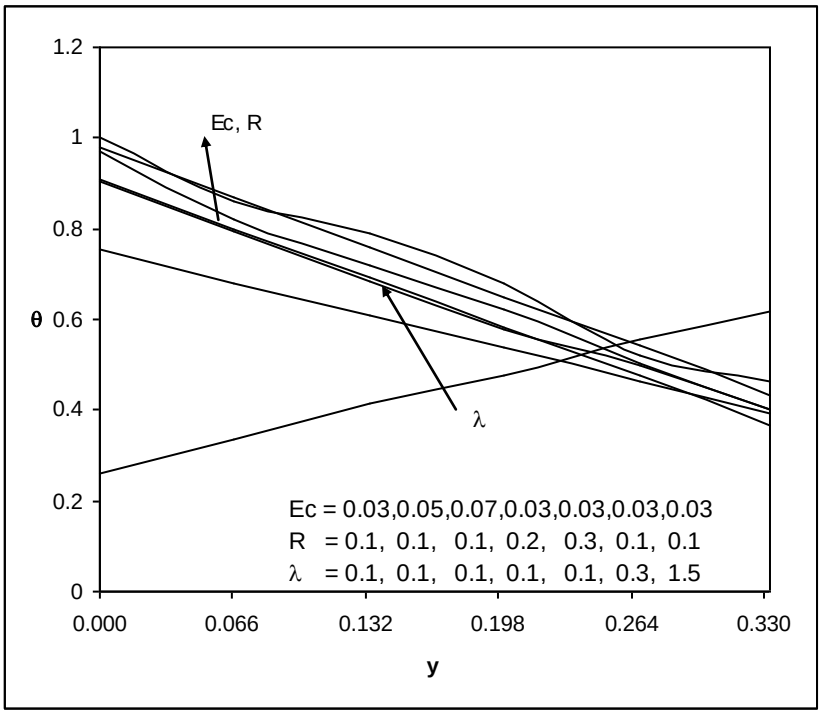

Fig. 23: Variation of C with Ec, R, λ at $x = \frac{1}{3}$ level

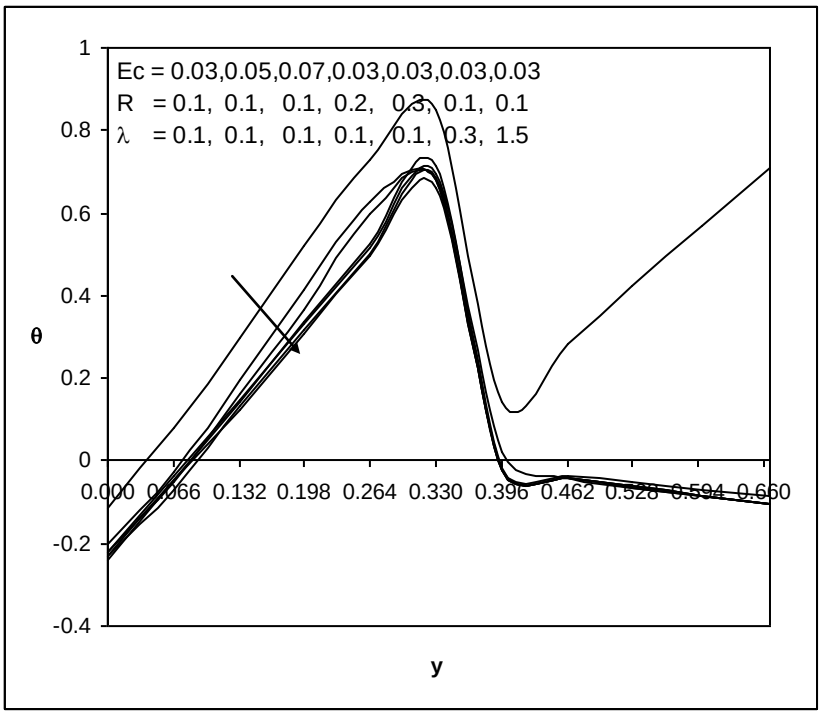

Fig. 24: Variation of C with Ec, R, λ at $x = \frac{2}{3}$ level

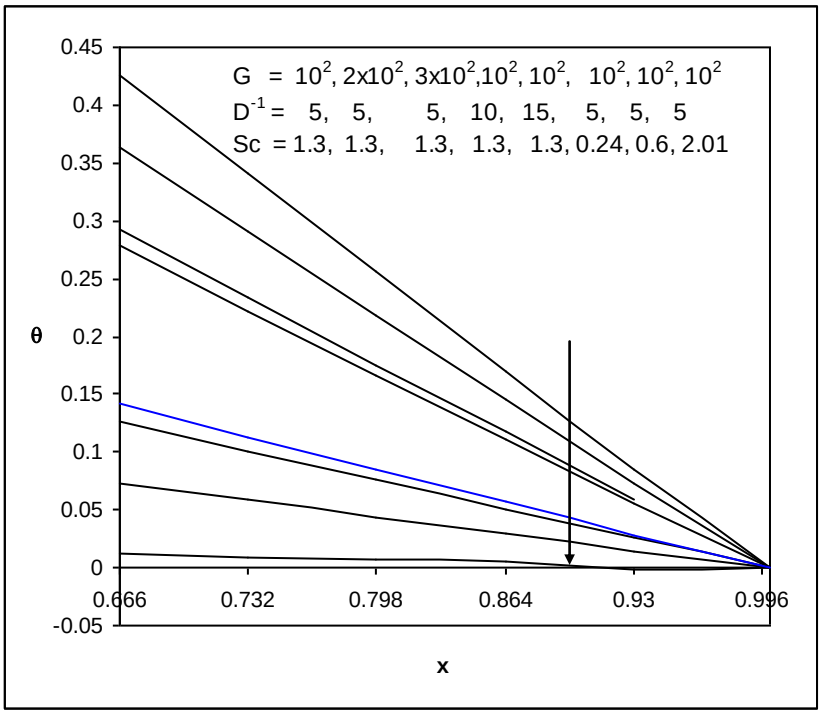

Fig. 25: Variation of N with G, D^{-1}, Sc at $y = \frac{2h}{3}$ level

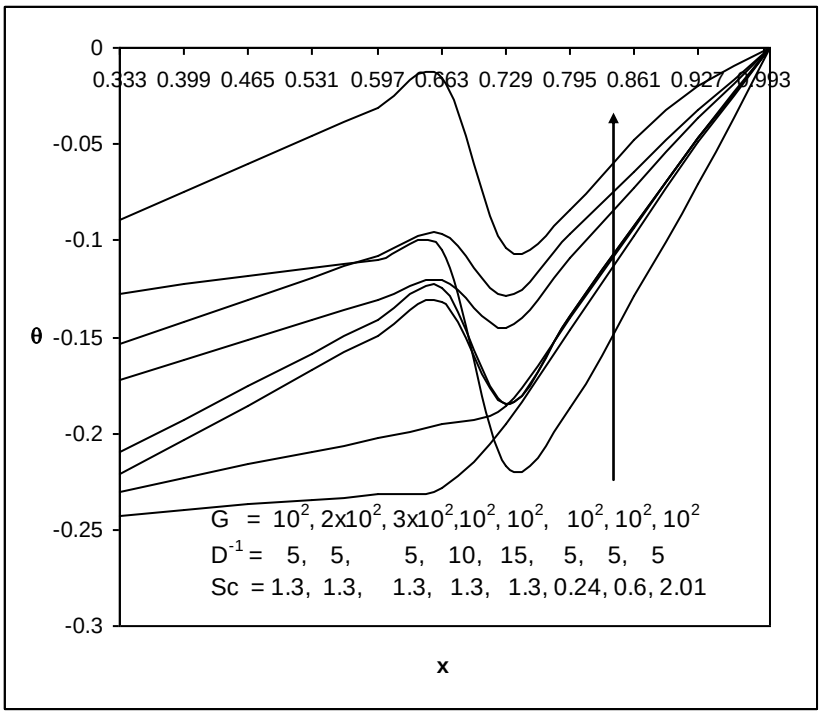

Fig. 26: Variation of N with G, D^{-1}, Sc at $y = \frac{h}{3}$ level

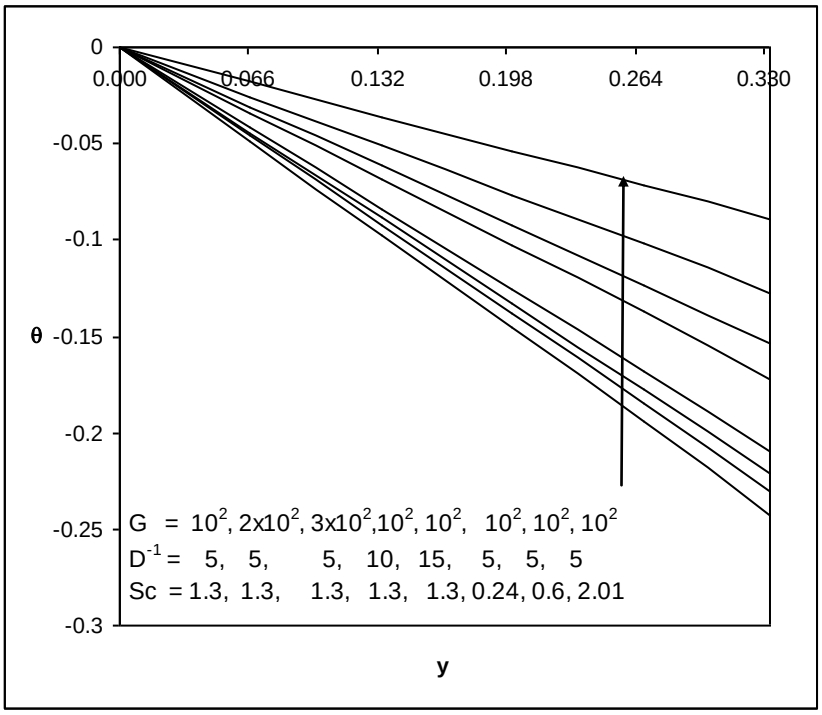

Fig. 27: Variation of N with G, D^{-1}, Sc at $x = \frac{1}{3}$ level

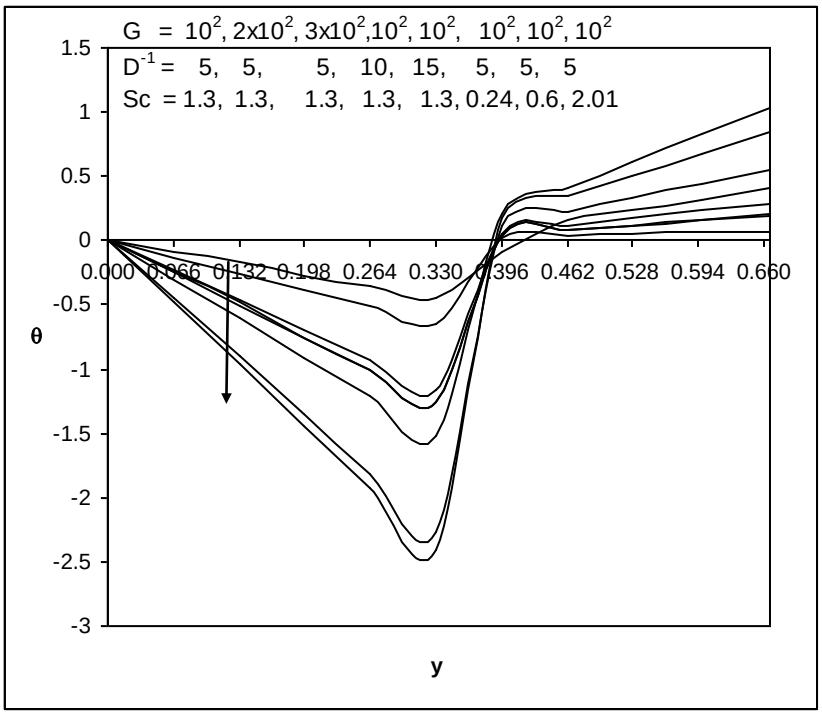

Fig. 28: Variation of N with G, D^{-1}, Sc at $x = \frac{2}{3}$ level

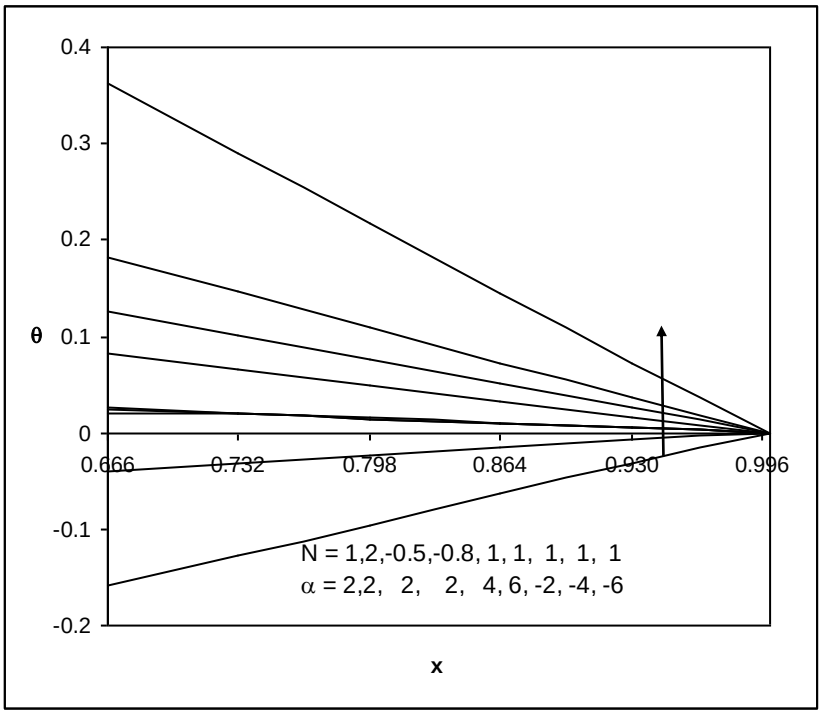

Fig. 29: Variation of N with N, α at $y = \frac{2h}{3}$ level

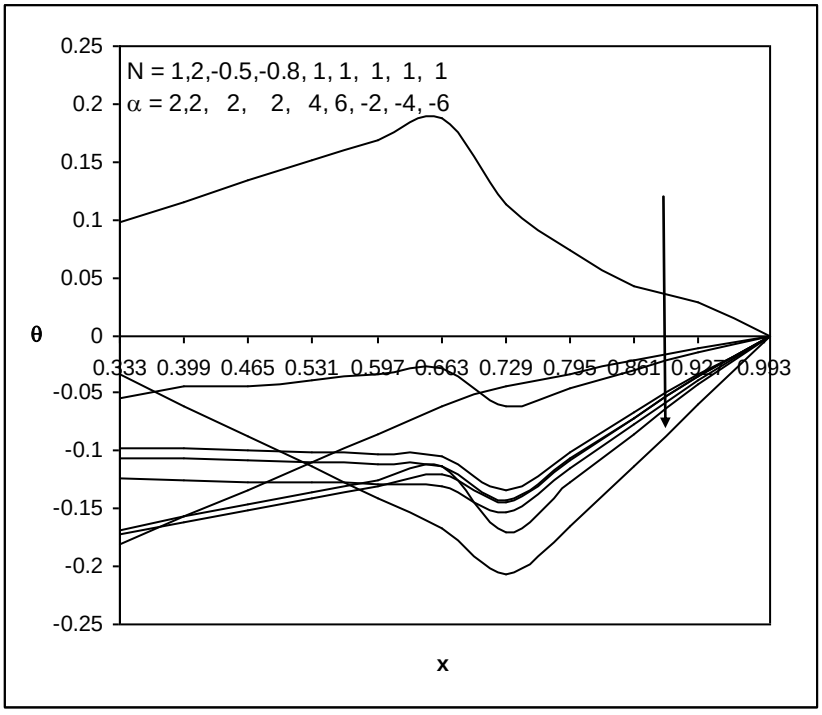

Fig. 30: Variation of N with N, α at $y = \frac{h}{3}$ level

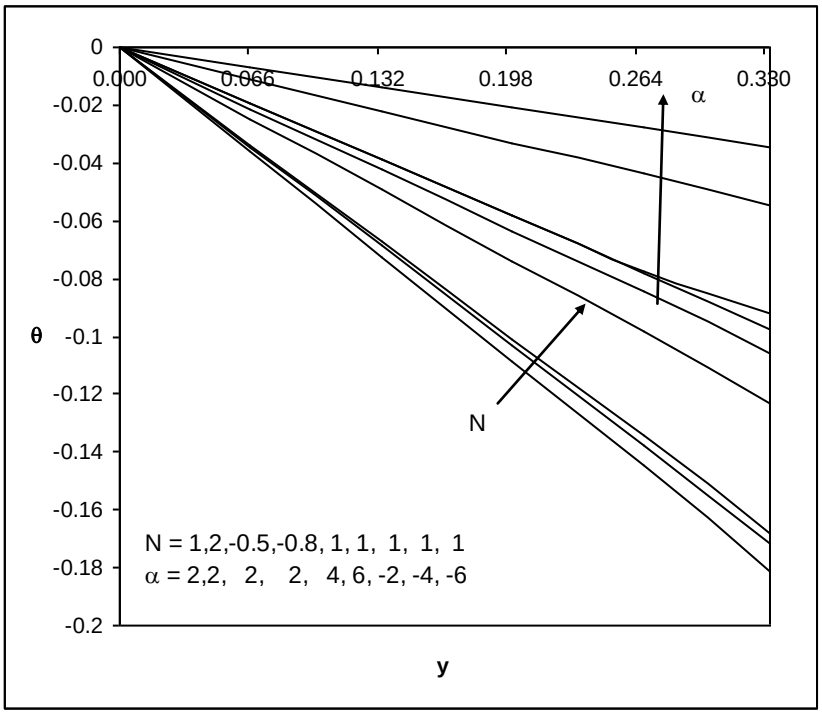

Fig. 31: Variation of N with N, α at $x = \frac{1}{3}$ level

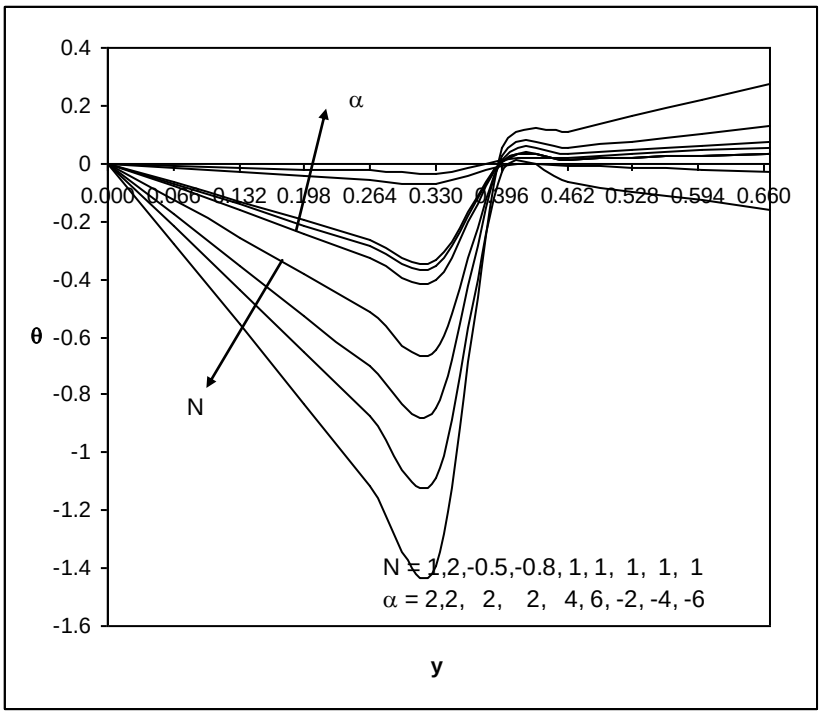

Fig. 32: Variation of N with N, α at $x = \frac{2}{3}$ level

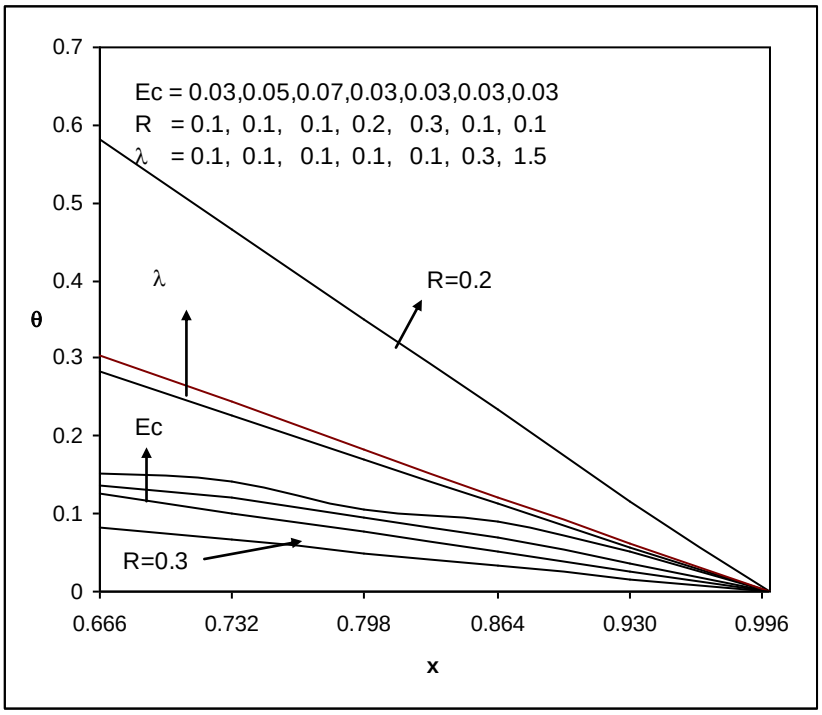

Fig. 33: Variation of N with Ec, R, λ at $y = \frac{2h}{3}$ level

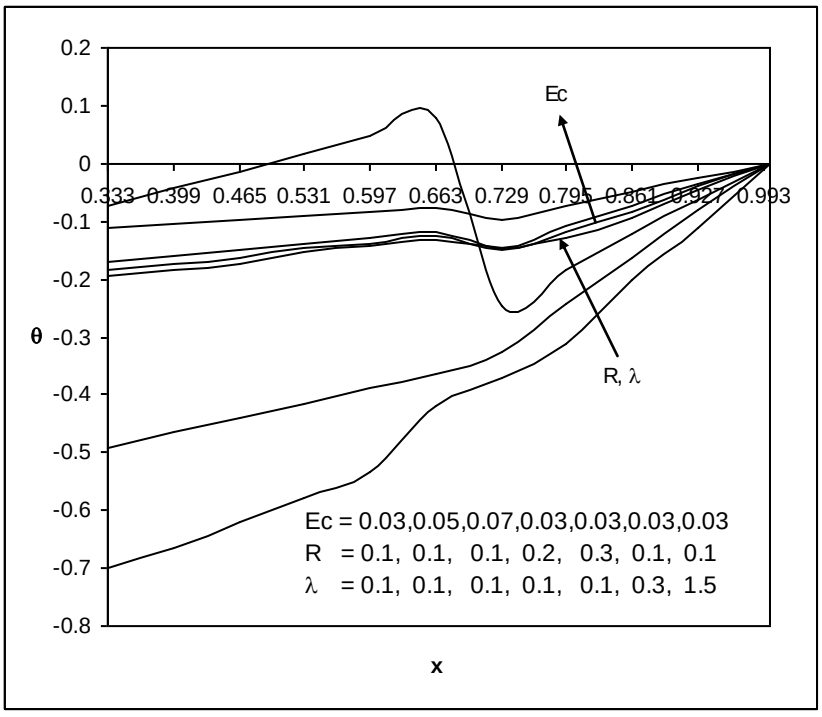

Fig. 34: Variation of N with Ec, R, λ at $y = \frac{h}{3}$ level

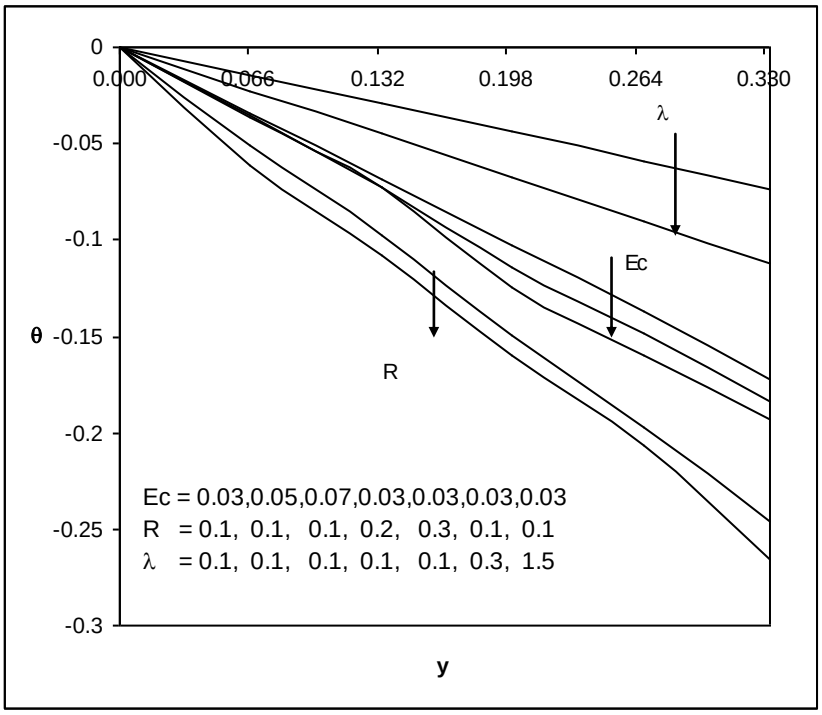

Fig. 35: Variation of N with Ec, R, λ at $x = \frac{1}{3}$ level

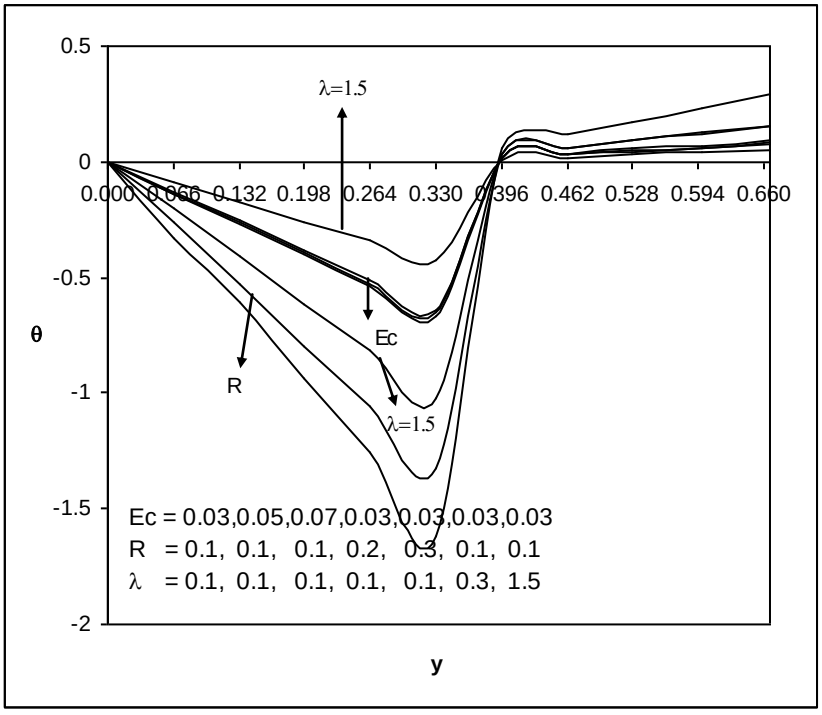

Fig. 36: Variation of N with Ec, R, λ at $x = \frac{2}{3}$ level

The rate of heat transfer (Nusselt number) on the side x = 1 is shown in tables 1-3 for different values of D^{-1},α, N, Sc, Ec, λ & R. We find that the rate of heat transfer on the lower and upper quadrants reduces with increase in G and D^{-1}, while on the middle quadrant |Nu| enhances with increase in G or D^{-1}. The variation of Nu with micro polar parameter R shows that an increase $R \leq 0.2$ enhances the Nusselt number on all the three quadrants, while for higher $R \geq 0.3$, it depreciates on the lower quadrant and enhances on the middle and upper quadrants. With reference to spin gradient parameterλ, we find that |Nu| reduces with λ on all three quadrants (table 1). The variation of Nusselt number with heat source parameter α shows that |Nu| reduces with α on the lower quadrant and enhances on the middle and upper quadrants and an increase in the strength of heat absorbing source leads to an enhancement in |Nu| on all three quadrants. With respect to Ec, we find that higher the dissipation heat larger |Nu| on all the three quadrants. The variation of Nu with buoyancy ratio 'N' shows that when molecular buoyancy force dominates over the thermal buoyancy force, the rate of heat transfer reduces irrespective of the directions of buoyancy forces (table (3).

The variation of Nu with Sc shows that lesser the molecular diffusivity ($Sc \leq 0.6$) smaller |Nu| on lower and upper quadrants and larger on the middle and for further lowering of molecular diffusivity ($Sc \geq 1.3$) larger |Nu| on all the quadrants and for still lowering of the molecular diffusivity ($Sc \geq 2.01$) |Nu| enhances on the lower and middle quadrants and reduces on the upper quadrant (table 2).

The rate of mass transfer (Sherwood number (Sh) on the side x = 1, is shown in tables 4-6 for different parameter values. It is found that the rate of mass transfer on the lower and upper quadrants reduces with increase in G & D^{-1}, and an increase $G \leq 2$ & $D^{-1} \leq 10$ leads to depreciation in |Sh| on the middle quadrant while for higher $G \geq 3$ or $D^{-1} \geq 15$, we notice an enhancement in |Sh|. The variation of Sh with micro polar parameter R shows that |Sh| enhances on the lower and middle and reduces on the upper quadrant for $R \leq 0.2$ and for higher $R \geq 0.3$, |Sh| reduces on the lower and upper quadrants and enhances on the middle quadrant. With reference to spin gradient parameter λ we find that |Sh| enhances on the lower and upper quadrants and reduces on the middle quadrant (table 4).

The variation of Sh with buoyancy ratio 'N' shows that when molecular buoyancy force dominates over the thermal buoyancy force, the rate of mass transfer reduces on the lower and middle quadrants and enhances on the upper quadrant irrespective of the directions of buoyancy forces. With respect to Sc, we find that the rate of mass transfer enhances on the lower and middle quadrants and reduces on the middle with $Sc \leq 0.6$ and reduces for higher Sc = 1.3. An increase in $Sc \geq 2.01$ reduces |Sh| on all quadrants (table 5).The variation of Sh with heat source parameter α shows that |Sh| on the lower and upper quadrant enhances with $\alpha > 0$, and an increases in $|\alpha|$ enhances |Sh| on the lower and middle quadrants and reduces on the upper quadrant. With respect to Ec, we find that higher the dissipative heat larger |Sh| on the lower and upper quadrants and reduces on the middle quadrant (table 6).

The couple stress (C_w) on x = 1, is shown in tables 7-9 for different parameter values. It is found that the C_w on the middle quadrant enhances with increase in $G \leq 2$ or $D^{-1} \leq 10$ and reduces with higher $G \geq 3$ or $D^{-1} \geq 15$, while on the upper quadrant; the C_w reduces with G & D^{-1}. An increase in R enhances C_w on the middle quadrant and enhances on the upper quadrant. With respect to λ we notice that C_w reduces on the middle quadrant and enhances on the upper quadrant (table 7).The variation of C_w with the buoyancy ratio 'N' shows that when the molecular buoyancy force dominates over the thermal buoyancy force, C_w enhances on the middle quadrant and reduces on the upper quadrant when the buoyancy forces are in the same direction and for the forces acting in opposite directions, we notice a depreciation in $|C_w|$ on the middle and upper quadrants. With respect to Sc, we find that C_w reduces on the middle quadrant and enhances on the upper quadrant with increase in Sc (table 8).The variation of C_w with heat source parameter α shows that an increase $\alpha \leq 4$ enhances on the middle quadrant and reduces on the upper quadrant, while for higher $\alpha \geq 6$ we notice a depreciation in C_w on the middle quadrant and enhancement on the upper quadrant. An increase in the strength of the heat absorbing source ($\alpha \leq 0$) leads to a depreciation in C_w on both the quadrants. Also higher the dissipation heat larger the C_w on the middle and upper quadrants (table 9).

Table – 1
Nusselt Number at x = 1

	I	II	III	IV	V	VI	VII	VIII	IX	X
Nu_1	4.23062	4.445464	2.16268	3.476928	2.870577	3.48638	3.011929	4.270648	4.252964	4.2444412
Nu_2	-0.313492	-0.800912	7.5844	0.46636	0.714912	0.44752	0.47022	0.32068	0.31892	-0.295796
Nu_3	3.587732	3.367736	6.877	3.135372	2.771836	3.122076	2.852564	3.646452	3.609948	3.304552
R	0.1	0.2	0.3	0.1	0.1	0.1	0.1	0.1	0.1	0.1
G	10^2	10^2	10^2	$2x10^2$	$3x10^2$	10^2	10^2	10^2	10^2	10^2
D^{-1}	5	5	5	5	5	10	15	5	5	5
λ	0.1	0.1	0.1	0.1	0.1	0.1	0.1	0.5	1.5	5

Table – 2
Nusselt Number at x = 1

	I	II	III	IV	V	VI	VII
Nu_1	4.23062	3.739888	18.03376	1.23088	4.279596	4.16412	4.341556
Nu_2	-0.313492	0.143856	-2.2124	-0.907928	-0.10396	-0.197816	-0.392052
Nu_3	3.587732	3.40152	-4.5618	3.701552	3.86464	3.456284	3.51776
N	1	2	-0.5	-0.8	1	1	1
Sc	1.3	1.3	1.3	1.3	0.24	0.6	2.01

Table – 3
Nusselt Number at x = 1

	I	II	III	IV	V	VI	VII	VIII
Nu_1	4.23062	3.452648	0.08476	1.9231548	1.23036	0.787832	4.25928	4.26928
Nu_2	0.313492	1.368884	-10.53492	1.475168	0.957656	-0.582972	-0.337392	-0.347392
Nu_3	3.587732	4.910164	19.75596	1.25162	0.901824	0.657436	3.60388	3.62388
α	2	4	6	-2	-4	-6	2	2
Ec	0.03	0.03	0.03	0.03	0.03	0.03	0.05	0.07

Table – 4
Sherwood number (Sh) at x =1

	I	II	III	IV	V	VI	VII	VIII	IX	X
Sh_1	2.92756	2.957184	2.452456	2.844332	2.571332	2.838972	2.627792	2.87516	2.923492	2.926676
Sh_2	-0.73256	-0.865076	-0.95868	0.004192	0.521504	0.015348	0.207428	-0.786908	-0.720244	-0.71494
Sh_3	2.419748	2.349976	-0.837484	2.385090 4	2.309686 8	2.379451 2	2.316511 2	2.423884	2.425212	2.4311
R	0.1	0.2	0.3	0.1	0.1	0.1	0.1	0.1	0.1	0.1
G	10^2	10^2	10^2	$2x10^2$	$3x10^2$	10^2	10^2	10^2	10^2	10^2
D^{-1}	5	5	5	5	5	10	15	5	5	5
λ	0.1	0.1	0.1	0.1	0.1	0.1	0.1	0.5	1.5	5

Table – 5
Sherwood number (Sh) at x =1

	I	II	III	IV	V	VI	VII
Sh_1	2.92756	2.87138	2.1291572	1.285128	3.169424	3.24714	2.658196
Sh_2	-0.73256	-0.29384	-3.5408	-0.284008	-3.51908	-1.977964	0.298544
Sh_3	2.419748	2.438928	-0.127112	2.71452	0.452388	2.60730944	2.2528428
N	1	2	-0.5	-0.8	1	1	1
Sc	1.3	1.3	1.3	1.3	0.24	0.6	2.01

Table – 6
Sherwood number (Sh) at x =1

	I	II	III	IV	V	VI	VII	VIII
Sh_1	2.92756	3.107556	3.208556	3.102016	3.157228	3.202524	2.93652	2.93752
Sh_2	-0.73256	-0.438788	-0.248376	-0.817008	-0.887884	-0.934416	-0.723536	-0.713636
Sh_3	2.419748	2.50834	2.6761488	2.561924	2.561108	2.555248	2.42092	2.43192
α	2	4	6	-2	-4	-6	2	2
Ec	0.03	0.03	0.03	0.03	0.03	0.03	0.05	0.07

Table – 7
Cw at x = 1

	I	II	III	IV	V	VI	VII	VIII	IX	X
Cw_1	2	2	2	2	2	2	2	2	2	2
Cw_2	4.567696	7.30624	10.40996	7.01796	3.798936	7.01144	6.64132	6.0934	3.71354	2.512556
Cw_3	1.700540 8	1.3774	0.836768	1.228376	0.384756	1.188864	0.8435	1.386496	1.8027224	1.9414072
R	0.1	0.2	0.3	0.1	0.1	0.1	0.1	0.1	0.1	0.1
G	10^2	10^2	10^2	$2x10^2$	$3x10^2$	10^2	10^2	10^2	10^2	10^2
D^{-1}	5	5	5	5	5	10	15	5	5	5
λ	0.1	0.1	0.1	0.1	0.1	0.1	0.1	0.5	1.5	5

Table – 8
Cw at x = 1

	I	II	III	IV	V	VI	VII
Cw_1	2	2	2	2	2	2	2
Cw_2	4.567696	5.513808	6.34952	2.1261428	6.0453	5.6151	4.2624
Cw_3	1.7005408	1.487428	2.6366	1.7731	-0.1915	-1.4028	-2.1270
N	1	2	-0.5	-0.8	1	1	1
Sc	1.3	1.3	1.3	1.3	0.24	0.6	2.01

Table – 9
Cw at x = 1

	I	II	III	IV	V	VI	VII	VIII
Cw_1	2	2	2	2	2	2	2	2
Cw_2	4.567696	7.56724	2.2736208	3.618372	3.424992	3.322752	4.57604	4.576648
Cw_3	1.7005408	0.904964	2.1045608	1.8727744	1.8707804	1.8696884	1.70204	1.7026372
α	2	4	6	-2	-4	-6	2	2
Ec	0.03	0.03	0.03	0.03	0.03	0.03	0.05	0.07

REFERENCES

[1] BORN, P.J, CHOW, L.C and TIEN, C.L:Int. J. Heat Transfer 20, 919 (1977).
[2] BEJAN, A and TIEW, C.L: Trans, ASME, J. Heat Transfer 100, 191 (1978).
[3] CATTON, I: Natural convection in enclosure, Proc. 6th int. Heat Transfer conf. Toranto, Canada. Vol. 6. pp 13-31 (7-11 August 1978).
[4] CATTON, I: Int. J. Heat Mass Transfer 15, 665 (1972).
[5] CLIFFE, K.A and WINTER, K.H: Numerical methods for predicating preferred and anomalous flows in Benard convection. Proc. 6th Int. conf-numerical methods in Thermal problems (1989).
[6] CHA, O-KAUNG CHEN and TSAN – HUIHSO; Natural convection of micropolar fluids in a Rectangular Enclosure: Int. J. Engng sci. vol. 34. 4. pp. 407-415(1966).
[7] DAVIS, S.H: J. Fluid mech. 30. 465 (1967).
[8] ELDER.J.M: J. fluid Mech 27, 29 (1967).
[9] ERINGEN, A.C: Int. J. Engng sci 2, 205 (1964).
[10] ERINGEN, A.C: J. Math Mech 16 1 (1077).
[11] ERINGEN, A.C:J. Math Anal. Appl 38, 480 (1972).
[12] HAAJIZADEH, M and TIEN, C.L: Trans ASME, J. Heat Transfer 105, 803 (1978).
[13] JENA, S.K and BHATTACHARYA, S.P Int. J. Engng sci, 24, 69 (1986).
[14] KIMURA, S and BEJAN, A: Phy, fluids 28 2980 (1985).
[15] KIM, D.M and VISKANTA, R: Trans, ASME, J. Heat Transfer 107, 139 (1985).
[16] NOVEMBER, M and NANSTEEL.M.W: Int. J. Heat Mass Transfer 30, 2433 (1987).
[17] OSTRACH, S: Adv, Heat Transfer 8, 161 (1972).
[18] OZOE, H, YAMAMTOTO, K, SAYAMA, H and CHURCHILL, S.W:Int. J. Heat Mass Transfer 17, 1209 (1972).
[19] OZOE, H and SAYAMA, H: Int. J. Heat Mass Transfer 18, 1425 (1975).
[20] SAMUELS, M.R and CHURCHILL, S.W: Alche. J. 10. 110 (1967).
[21] WALKER.K.L and HOMSY, G.M: J. fluid Mech. 87. 449 (1978).
[22] WILSON, G.L and RYDIN,R.A:Int. J. Numer. Mech. Fluids 10, 35 (1990).
[23] WANG, M, TSUJI,T, NAGANA,Y: Mixed convection with flow reversal in the thermal entrance region of horizontal and vertical pipes. Int. J. Heat Mass Transfer 37 (1994) 2305-2319.
[24] WANGmM, TSAN – HUISHU: Int. J. Heat and mass transfer 43 (2000) 1563-1572.